Simulation Modelling Practice and Theory 144 (2025) 103177

Contents lists available at ScienceDirect

Simulation Modelling Practice and Theory

journal homepage: www.elsevier.com/locate/simpat

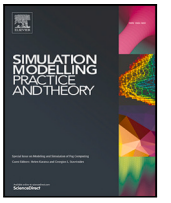

Mastering the complexity: An enhanced cellular automata-based framework for simulating resilience of hospital Power-Water-Firefighting-Space nexus system

Renlong Wang [a,b], Lingzhi Li [a,c,*], Wenjie Lin [a,c], Endong Wang [d], Jingfeng Yuan [e]

[a] Research Center of Smart City, Nanjing Tech University, Nanjing, 211816, China
[b] School of Emergency Management Science and Engineering, University of Chinese Academy of Sciences, Beijing, 100049, China
[c] College of Civil Engineering, Nanjing Tech University, Nanjing, 211816, China
[d] Construction Management and Engineering Division, State University of New York (SUNY ESF), Syracuse, 13210, United States
[e] Department of Construction and Real Estate, School of Civil Engineering, Southeast University, Nanjing, 211189, China

ARTICLE INFO

Keywords:
Hospital
Power-Water-Firefighting-Space (PWFS) system
Resilience assessment
Cellular automata
Interdependency
COVID-19

ABSTRACT

Modeling the resilience of hospital Power-Water-Firefighting-Space (PWFS) nexus systems is a complex, dynamic, and nonlinear challenge characterized by high uncertainty. Existing methods, mainly agent-based and network-based models, face difficulties in balancing detailed component-level behaviors with broader system-level interdependencies and neglect the impact of external disruptions, such as surges in service demand during the COVID-19 pandemic, on hospital PWFS system resilience. To address this, the study proposes an enhanced cellular automata (CA)-based framework for simulating hospital PWFS system resilience. The PWFS system is modeled as a seven-tuple CA, incorporating cell structure, state, space, neighborhood, transition rules, and time, facilitating the integration of micro-level component behavior with macro-level interdependencies. A set of resilience metrics, including robustness, rapidity, performance loss, and an integrated resilience index, are introduced, based on the system performance curve, which includes normality, connectivity, resource transfer efficiency, and space functionality. The model enables scalable, polynomial-time simulations of cascading failures, resource redistribution, and spatial–temporal recovery across interconnected PWFS subsystems. A real-world outpatient building case study demonstrates the applicability and validity of the enhanced CA model. The findings emphasize the importance of modeling intra-system interdependencies and provide actionable insights for infrastructure design and emergency preparedness. Overall, the enhanced CA framework offers a systematic, scalable, and computationally efficient approach to resilience assessment, bridging theoretical modeling with practical infrastructure planning.

1. Introduction

In high-risk society, healthcare facilities face constant threats from extreme events such as severe weather, epidemics, and conflicts [1]. As critical emergency infrastructure, hospitals must maintain and enhance their functionality to ensure uninterrupted healthcare services [2,3]. Consequently, the concept of resilience has emerged in engineering to address challenges posed by various

* Correspondence to: 30 South Puzhu Road, Nanjing 211816, Jiangsu Province, China.
E-mail addresses: wangrenlong23@mails.ucas.ac.cn (R. Wang), 6370@njtech.edu.cn (L. Li), 202361226143@njut.edu.cn (W. Lin), ewang01@esf.edu (E. Wang), jingfeng-yuan@seu.edu.cn (J. Yuan).

https://doi.org/10.1016/j.simpat.2025.103177
Received 19 July 2024; Received in revised form 20 May 2025; Accepted 27 June 2025
Available online 8 July 2025

disruptions [4]. Many studies in engineering define resilience as the ability of system to resist, absorb, and recover quickly from disturbances [5]. It is clear that an ability of hospital to operate during disruptions relies heavily on essential lifeline systems, such as power, water supply, and firefighting systems [6]. These systems are not independent but intricately interconnected, which increases the vulnerability of hospital, even a minor issue could trigger cascading failures across the entire system [7,8]. Moreover, functional units within the hospital, such as admission rooms, surgery rooms, and wards, act as the bridge between lifeline systems and end-users, making the hospital a typical socio-technical system. Thus, this study focuses on the Power-Water-Firefighting-Space (PWFS) nexus system for resilience evaluation and evolutionary analysis, adopting a perspective based on the coupling of socio-technical systems.

Modeling the hospital PWFS system for resilience simulation is a complex, dynamic, and nonlinear problem, marked by significant uncertainty [9]. The quantitative assessment of hospital resilience, based on system performance, involves two main steps: system performance simulation and resilience metric extraction. Currently, hospital performance simulation primarily uses agent-based and network-based methods to model the temporal evolution of system performance, such as availability, productivity, and service quality, in response to external disturbances (i.e., resilience curve) [10,11]. The agent-based method models the behavior of individual components within the system, addressing cascading failures, self-adaptation, and decision-making, and captures emergent phenomena from the bottom up [12–14]. The network-based approach, on the other hand, represents the macro topology of system using network connections, making it a mainstream method for resilience simulation due to its intuitive representation and ease of computation [15,16]. Key features, such as robustness, rapidity, and performance loss, are then extracted from the resilience curve to characterize resilience [17]. However, agent-based models depend heavily on behavioral assumptions, where even small variations in agent behavior can significantly impact outcomes, making their validity contingent on these assumptions. Most network-based studies on hospital resilience focus on macro-level topologies between hospitals, often overlooking internal dynamics and component-level changes within individual hospitals. Furthermore, current research tends to emphasize service performance disruptions, neglecting the impact of external shocks, such as COVID-19 demand surges, on the resilience of critical hospital systems like power, water, and space utilization, which are essential for infrastructure design.

This study proposes a resilience simulation framework for the hospital PWFS nexus system, employing advanced cellular automata (CA) to assess its resilience. With the enhanced CA model, the PWFS system is modeled as a seven-tuple cellular automaton, based on a detailed analysis of its composition and operational dynamics. A set of performance metrics, considering system functionality and topology, is introduced, with the robustness, rapidity, performance loss, and an integrated indicator to evaluate the resilience of the PWFS system to external disturbances and its recovery capacity. The main contributions of this study are summarized as follows:

- Methodology: This study presents an enhanced seven-tuple CA model, comprising components of cell, cellular property, cellular space, cellular state, cellular neighborhood, transition rules, and time step, for evaluating the resilience of the PWFS system, which is a novel extension of the traditional CA model for PWFS system modeling. Unlike conventional ABM- and network-based methods, the proposed enhanced CA model integrates macro-level interdependencies, captured in network-based models, and micro-level component behaviors, emphasized in agent-based models, offering a more comprehensive framework that combines the strengths of both approaches. Additionally, the multiplicative aggregated resilience measurement is comparable across scenarios and systems, with a proven linear sensitivity to performance aggregation.
- Practice: This study introduces the enhanced CA model, a scalable polynomial-time simulation framework for resilience evaluation, enabling effective modeling of complex systems under various conditions, making it well-suited for large-scale infrastructure resilience simulations. The case study further underscores the critical role of system interdependencies in resilience, offering valuable insights for the design of more robust and adaptable hospital infrastructure.

The remainder of this paper is organized as follows: Section 2 reviews the relevant literature. Section 3 introduces the enhanced CA-based method for the resilience assessment of the hospital PWFS system. Section 4 presents a case study of the NJHTCM outpatient building to demonstrate the proposed model, with model validation under the COVID-19 epidemic, various model settings, and comparisons with other methods. Section 5 offers conclusions and future research directions.

2. Literature review

Infrastructure resilience assessment is vital for improving infrastructure resilience. It can be divided into two primary types: qualitative and quantitative. This study focuses on quantitative assessment. Qualitative assessments often use conceptual frameworks to establish indicators for resilience evaluation, incorporating extensive knowledge and experience to conduct a quantitative analysis based on established theories such as 4Rs [18], PEOPLES [19], and DROP [20]. In contrast, quantitative resilience assessment involves extracting characteristic indicators from the time evolution curve of system performance after disturbance, reflecting the resilience level of the infrastructure [21]. Methods for measuring resilience curves emphasize rapidity, robustness, performance loss, and recovery capability [22]. However, challenges remain, particularly in developing standardized or universally applicable measures to quantify resilience across different hazards and environments [13]. This complicates comparisons between systems, especially those with interconnected dependencies, such as the PWFS system in this study.

The primary challenge in quantitatively assessing system performance resilience lies in developing effective modeling and simulation methods to accurately represent the evolution of system performance, such as availability, productivity, and service quality, over time under external disturbances [23,24]. Specifically, quantifying resilience in socio-technical systems like hospitals presents a complex issue, involving the representation of interdependencies among subsystems and uncertainties in

disturbances [25]. This requires a modeling approach capable of simulating the nonlinear dynamic evolution of systems with coupled effects. Currently, hospital system performance modeling and simulation methods primarily include agent-based and network-based approaches. The agent-based modeling (ABM) approach to hospital resilience focuses on individual-level behaviors rather than the overall system [26–28]. As a bottom-up method, it examines emergent system phenomena by simulating the autonomy, adaptation, and responses of individual agents [29]. This approach begins with individual behavior to analyze system behavior, aligning with the inherent dynamics of complex systems [30]. ABM has been applied across various hospital resilience areas, including evacuation planning [15], emergency medical response resilience [31,32], hospital-linked system resilience [33], and community resilience [34]. In network-based approaches, the critical facilities or infrastructures can be depicted as nodes, and their interdependencies as links in the network [35]. The modeling approach emphasizes the macro interdependence (e.g., topological structure and broadly-defined resources flow), which can be intuitively represented by the link of the network and analyzed through graph theory. Current performance simulation of hospital systems using network-based approaches primarily focuses on the resilience analysis of transportation networks created by multi-hospital casualty transfer points at the city level [17,31,36]. System resilience is typically evaluated by using a combination of network topology metrics (e.g., maximum connected subgraphs) [37], facility-oriented physical attribute metrics (e.g., facility accessibility) [16], and system performance metrics [38].

However, ABM relies on numerous behavioral assumptions, where small variations in agent behavior can lead to significant deviations in system outcomes. The validity and applicability of such models therefore hinge heavily on the accuracy of these assumptions [30]. On the other hand, most existing network-based studies on hospital resilience primarily focus on macro-level topological structures – often between multiple hospitals – while overlooking the internal dynamics and component-level functional changes within a single hospital system [39]. Moreover, much of the current research tends to concentrate solely on the impact of disruptions on healthcare service performance, neglecting how external shocks – particularly surges in demand for critical services, such as during the COVID-19 pandemic – affect the resilience of the hospital lifeline systems. Yet, these demand-driven disruptions can significantly influence the performance and recovery of interdependent systems such as power, water, and space utilization, offering crucial insights for designing more resilient hospital infrastructure. To address the limitations of existing approaches, this study proposes a CA-based simulation method that simultaneously considers macro-level interdependencies – captured in network-based models – and micro-level component behaviors — emphasized in agent-based models. While agent-based models excel at representing autonomous actions of individual agents, they often depend heavily on behavioral assumptions. Network-based methods, though effective in illustrating system-wide topological structures, generally overlook dynamic functional changes within hospitals. In contrast, the proposed CA framework integrates both dimensions in a unified, rule-based structure, enabling dynamic simulation of cascading failures and performance degradation across interconnected subsystems in hospital PWFS networks.

3. Methodology

3.1. Preliminaries of Cellular automata

Cellular automata (CA) is initially conceived by Von Neumann during the 1950s [40]. CA represents a discrete-space and discrete-time framework, wherein the spatial arrangement is depicted through a regular grid or latticed space, which may exist in one, two, or even higher dimensions. The traditional CA model mainly includes the elements of cellular space $\mathcal{L}$, cellular state $\mathcal{S}$, cellular neighborhood $\mathcal{N}$, and cellular transition rule $\mathcal{F}$, which can be represented by a four-tuple set [41]:

$$\mathcal{CA} := \{\mathcal{L}, \mathcal{S}, \mathcal{N}, \mathcal{F}\}. \tag{1}$$

The individual cells possess discrete states, expressed either as binary values or continuous values, to represent distinct features or attributes. Through localized transition rules, each cell autonomously updates its state based on the states of its neighboring cells, whereby these transition rules can exhibit determinism or stochasticity. Synchronously, at each time step, all cells update their states collectively and compute the subsequent state for the succeeding time step. Despite the seemingly straightforward nature of these rules, CA effectively exhibits intricate behaviors, such as self-organization, pattern formation, as well as asynchronous and synchronous oscillations [42]. CA demonstrates highly adaptable system behavior by iteratively applying simple local transition rules and showcases a broad range of potential applications. It captures the complexity of dynamic systems by constructing individual features in a "bottom-up" manner. By dividing the system into cells and defining their states and transition rules, it becomes possible to simulate the evolution of the entire system. Additionally, in contrast to complex differential equation models, CA necessitates only uncomplicated local transition rules without the need for complex equation solving [43].

3.2. Cellular automata modeling of power-water-firefighting-space system

This section presents the enhanced CA model for modeling the PWFS system, with the key component being the interdependence characterization and the transition rules of facilities within the system. This study extends the traditional four-tuple CA model into a seven-tuple set for the PWFS system, including *cell* $\mathcal{C}$, *cellular property* $\mathcal{P}$, *cellular space* $\mathcal{L}$, *cellular state* $\mathcal{S}$, *cellular neighborhood* $\mathcal{N}$, *transition rule* $\mathcal{F}$, and *time step* $\mathcal{T}$, as shown in Eq. (2) and Fig. 1.

$$\mathcal{CA} := \{\mathcal{C}, \mathcal{P}, \mathcal{L}, \mathcal{S}, \mathcal{N}, \mathcal{F}, \mathcal{T}\}. \tag{2}$$

The enhanced seven-tuple CA model builds upon the traditional four-tuple structure by adding new parameters to more effectively capture the dynamic evolution of the resource-driven PWFS system. This model is designed based on the operational practices

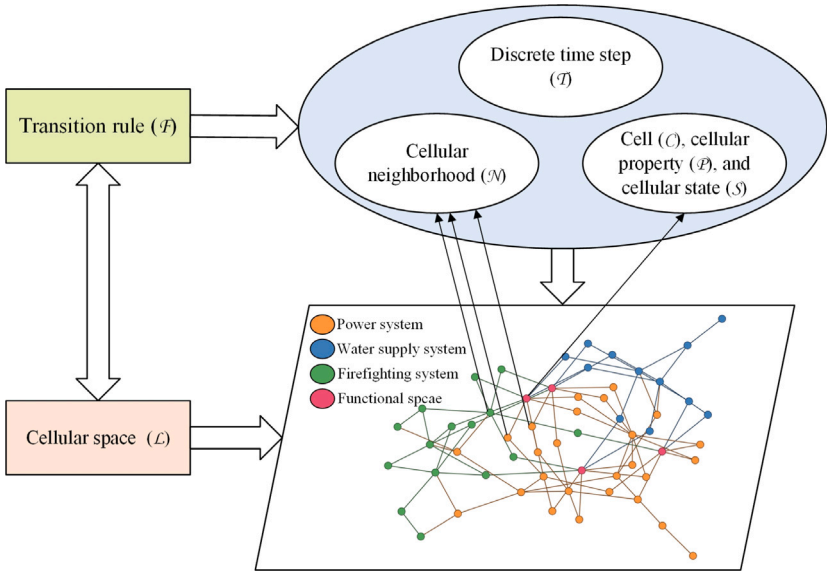

Fig. 1. Enhanced CA model of the PWFS system.

of the PWFS system, ensuring that it accurately reflects real-world behavior and provides valuable insights for managing and optimizing the system in dynamic environments. Specifically, the seven-tuple structure incorporates factors such as resource flow, topological changes, and local unit state evolution, offering a more detailed representation of interactions and resource flows within the PWFS system. Compared to the traditional four-tuple model, this enhanced version allows for a more comprehensive simulation of system behavior, particularly in complex systems with interdependent resources and components. This representation is essential for understanding cascading effects, fault propagation, and the intricate dynamics of resource flows in such systems.

The following basic elements of the enhanced CA model for the PWFS system are first introduced, including *cell*, *cellular property*, *cellular state*, and *time step*, which lay the groundwork for defining the rest components of the model. Let $\mathcal{I} := \{1, \ldots, I\}$, indexed by i, and $\mathcal{J} := \{1, \ldots, J\}$, indexed by j, denote the sets of cells and resources in the PWFS system, respectively.

Cell (C) represents the basic components of the PWFS system, categorized into power, water supply, firefighting, and functional space. Based on resource flow (i.e., power and water) within the system, cells are further classified as supply, transfer, and demand cells. The supply cells include the initial components that provide power or water, such as the municipal water system and distributed power generators. Transfer cells are responsible for resource conveyance, including distribution cabinets in the power system and pumps in the water supply system. Demand cells refer to the final components that consume resources, such as lighting fixtures in the power system and automatic sprinklers in the firefighting system.

Cellular property ($\mathcal{P}$) represents the resource characteristics of cells, including resource type, function type, and the actual and maximum workload for specific resources. Let the number of cells in the enhanced CA model of the PWFS system be m and the number of resource species be n. Thus, the cellular property P_{ij} of cell i for resource j is defined as:

$$P_{ij} = \{RT_{ij}, RFT_{ij}, RAWL_{ij}, RMWL_{ij}\}, \quad \forall i \in \mathcal{I}, j \in \mathcal{J}, \tag{3}$$

where RT_{ij} represents the type of resource possessed by cell i ($RT_{ij} = 1$ indicates cell i has resource j, otherwise $RT_{ij} = 0$), RFT_{ij} denotes the function type of cell i for resource j ($RFT_{ij} = -1$ indicates cell i inputs resource j, $RFT_{ij} = 0$ indicates cell i transfers resource j, and $RFT_{ij} = 1$ indicates cell i outputs resource j), $RAWL_{ij}$ represents the actual workload of cell i for resource j, and $RMWL_{ij}$ denotes the maximum workload of cell i for resource j. Let $RMT_{ij} = \lambda RMWL_{ij}$ for $0 < \lambda \leq 1$ denote the minimum resource threshold required for cell i to function, and $RDT_{ij} = \kappa RMWL_{ij}$ for $\kappa > 1$ represent the threshold for component overload damage. To simplify the discussion, let $\mathcal{I}_{ST}^{FT}$ denote the set of cells with system type $ST = p, w, f, s$ for power, water, firefighting, and functional space, and functional type $FT = s, t, d$ for supply, transfer, and demand, respectively, with the corresponding number of I_{ST}^{FT}. Let $\mathcal{J}_i^d$ denote the number and set of resource required by demand cell i.

Cellular state ($\mathcal{S}$) represents the operational condition of the cells. In this study, the cellular states S_i of cell $i \in \mathcal{I}$ are classified into four types, i.e., based on its behavior during the operation of the PWFS system: $S_i = -1$ indicates a damaged state with no resource when the component is damaged; $S_i = 0$ indicates a failure state with no input resources when the component is not damaged; $S_i = 1$ indicates a normal state, and $S_i = 2$ indicates an overloaded state.

Time step ($\mathcal{T}$) represents the unit discrete time during the response process of PWFS system under the simulated disturbance scenario.

Cellular space ($\mathcal{L}$) represents is the lattice space in which the cells of the enhanced CA model of the PWFS system are located. Resources in the PWFS system flow along physical associations and resource dependencies in the cellular space. For instance, the

hospital's electricity requirements are fulfilled by the municipal power system, which is then transmitted to electrical facilities (e.g., general lighting, fire detectors, and chillers) via transformer substations and distribution boxes. Similarly, the municipal water supply system transports water to water facilities (e.g., indoor fire hydrants, fire sprinklers, and domestic water amenities) through storage tanks and pumps. Notably, hospital water supply system and firefighting system rely on water as one of the most central resources. Therefore, this study integrates the water supply system and the firefighting system into a cohesive and homogeneous system referred to as the water-fire system. This terminology is adopted to encompass the transportation and utilization of the shared resource (i.e., water). Then, drawing upon the resource flows within the cellular space, a power cellular space with the dimensions of $I_p \times I_p$ and a water-fire cellular space with the dimensions of $I_v \times I_v$, where $I_v = I_w + I_f$, are established. The components within the power cellular space correspond to power facility components and electric circuits, while those within the water-fire cellular space represent hydraulic facility components and water network pipes.

Cellular neighborhood ($\mathcal{N}$) characterizes the interdependencies among the components within the PWFS system, which result from physical connections and resource interdependencies. The cellular neighborhood of all cells $i \in \mathcal{I}$ in the PWFS system is denoted by the adjacency matrix:

$$\mathbf{N} = \begin{bmatrix} \mathbf{A}_{I_p \times I_p} & \mathbf{B}_{I_p \times I_v} \\ \mathbf{C}_{I_v \times I_p} & \mathbf{D}_{I_v \times I_v} \end{bmatrix}_{I \times I}, \tag{4}$$

where $n_{i_1 i_2} = 1$ indicates the existence of a connection from cell i to cell j, otherwise $n_{i_1 i_2} = 0$, $\mathbf{A}_{I_p \times I_p}$ denotes the correlation matrix encompassing the interrelationships among the various components within the power system, $\mathbf{B}_{I_p \times I_v}$ represents the cross-domain correlation matrix extending from the power system to the water-fire system, $\mathbf{C}_{I_v \times I_p}$ represents the cross-domain correlation matrix from the water-fire system to the power system, and $\mathbf{D}_{I_v \times I_v}$ corresponds to the correlation matrix containing the interrelationships among the components within the water-fire system. The adjacency matrix $\mathbf{N}$ delineates the path of resource transfer, where electricity serves as the transferred resource in $\mathbf{A}_{I_p \times I_p}$ and $\mathbf{B}_{I_p \times I_v}$, while water functions as the transferred resource in $\mathbf{C}_{I_v \times I_p}$ and $\mathbf{D}_{I_v \times I_v}$. Let $\mathcal{N}_i := \{i_2 \in \mathcal{I} : \exists i_1 \in \mathcal{I}, n_{i_1 i} = 1, n_{i_1 i_2} = 1\}$ denote the set of neighboring cells of cell $i \in \mathcal{I}$, i.e, the set of cells that has the identical direct upstream cells of cell i. The adjacency matrix $\mathbf{M}$ can be generated using the improved Warshall method for $\mathbf{N}$. Thus, the set of parent and child cells of cell i are defined as $\overrightarrow{\mathcal{N}_i} := \{i_1 \in \mathcal{I} : m_{i_1 i} = 1\}$ and $\overleftarrow{\mathcal{N}_i} := \{i_1 \in \mathcal{I} : m_{i i_1} = 1\}$, respectively. This representation of cellular neighbors differs from the traditional set-based representation, breaking the limitation of cellular neighbors being confined to lattice adjacency.

The following cellular transition rules are crucial components of the enhanced CA model for the PWFS system, comprising three parts: the resource transition rule, the power cellular state transition rule, and the water-fire cellular state transition rule.

The resource transfer rule establishes the conditions for cellular resource transfer and the method for calculating changes in resource stock when disturbances occur. It is based on the fundamental principle of resource transfer (i.e., potential difference) derived from physics [44]. The core idea is that resources flow from cells with surplus (high potential) to those with demand (low potential), similar to physical systems (e.g., electricity or fluid dynamics), where energy or materials naturally move from regions of higher potential to lower potential. For any cells $i_1, i_2 \in \mathcal{I}$, they are identified as the demand and supply cells for resource $j \in \mathcal{J}$, respectively, if the following conditions hold:

$$RFT_{i_1 j} + RFT_{i_2 j} = 0 \wedge RFT_{i_1 j} = -1. \tag{5}$$

Resource transfer is feasible when the actual resource load difference for resource $j \in \mathcal{J}$ (referred to as the potential difference) between cells $i_1, i_2 \in \mathcal{I}$ satisfies the conditions in Eqs. (5) and (6):

$$d_{i_1 i_2 j} = RAWL_{i_2 j} - RAWL_{i_1 j} \geq 0, \tag{6}$$

where $d_{i_1 i_2 j}$ represents the potential difference in resource j between cells i_1 and i_2, meaning that resource transfer occurs only when the potential difference between supply and demand cells is positive.

Regarding the calculation of cellular resource stock, it is assumed that resource transfer within the PWFS system reaches a steady state during propagation, based on system theory, where stability is maintained by dynamically balancing resource distribution. The amount of resource j held by cell i at time $t+1$ depends on the resource stock of cell i at time t and the states of its neighboring cells at time $t+1$. Let $\mathcal{I}'$, indexed by i', represent the set of failed cells. The allocation of surplus capacity of cell $i \in \mathcal{I}$ at time t is defined as:

$$\Delta WL_{ii'jt} = RAWL_{i'jt} \times \frac{RAWL_{ijt}}{\sum_{i \in \mathcal{N}_{i'}} RAWL_{ijt}}, \quad \forall i' \in \mathcal{I}', i \in \mathcal{N}_{i'}, j \in \mathcal{J}, t \in \mathcal{T}, \tag{7}$$

where $\mathcal{N}_{i'}$ denote the set of neighboring cells of cell $i' \in \mathcal{I}'$, $RAWL_{i'jt}$ is the actual workload of the failed neighboring cell i' for resource j at time t, $RAWL_{ijt}$ represents the actual workload of cell i for resource j at time t, and $\sum_{i \in \mathcal{N}_{i'}} RAWL_{ijt}$ is the sum of the actual workload of neighboring cells of cell i' for resource j at time t. This equation ensures that the workload of the failed cell is fairly distributed among its operational neighbors in proportion to their current load, as these operational cells are most likely to have the capacity to absorb the additional load. The resource stock of cell $i \in \mathcal{I}$ at time $t+1$ is then computed as:

$$RAWL_{ijt+1} = RAWL_{ijt} + \sum_{i' \in \mathcal{I}'} \Delta WL_{ii'jt}, \quad i \in \mathcal{I}, j \in \mathcal{J}, t \in \mathcal{T} \backslash \{T\}, \tag{8}$$

where $\sum_{i' \in \mathcal{I}'} \Delta WL_{ii'jt}$ represents the amount of resources reallocated by cell i from failed neighboring cells at time $t+1$.

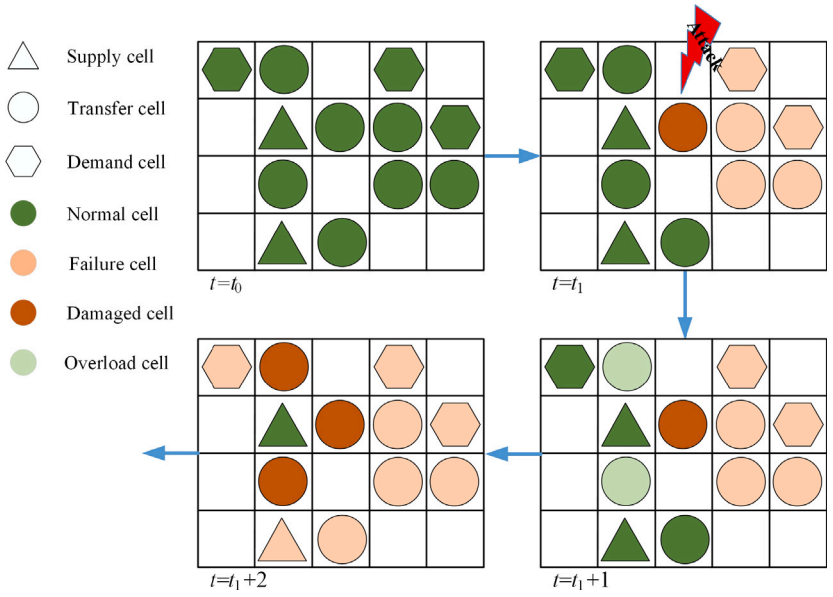

Fig. 2. Schematic diagram of cellular state transition.
Figure Note: At the initial state $t = t_0$, the system operates normally. At $t = t_1$, a cell is attacked and damaged, causing its sub-cells to fail. At $t = t_1 + 1$, the redistribution of the attacked cell's workload leads to an overload in its neighboring cells. At $t = t_1 + 2$, sustained overload in the neighboring cells causes damage, resulting in a total system failure downstream.

The power cell state transition rule models the dynamic behavior of power facilities, emphasizing the impact of cascading failures in an interconnected power system. This stems from the fact that, in the PWFS system, the power system generally acts as the upstream provider of essential energy to components such as water and firefighting systems, which rely on power to function properly [45]. The state of cell i at time $t + 1$ depends on its state at time t and the states of its neighboring cells at time t. The power cell state transition rule for any cell $i \in \mathcal{I}_p$ is defined as:

$$S_{it+1} = \begin{cases} -1, & \text{if } S_{t-M+1} = S_{t-M+2} = \cdots = S_t = 2, \\ 0, & \text{if } (RAWL_{ijt} < RMT_{ij}) \vee (S_{i'jt} = -1 \text{ or } 0, \forall i' \in \overrightarrow{\mathcal{N}}_i^p), \\ 1, & \text{if } (RMT_{ij} \le RAWL_{ijt} < RDT_{ij}) \wedge (S_{i'jt} = 1 \text{ or } 2, \forall i' \in \overrightarrow{\mathcal{N}}_i^p), \\ 2, & \text{if } (RAWL_{ijt} \ge RDT_{ij}) \wedge (S_{i'jt} = 1 \text{ or } 2, \forall i' \in \overrightarrow{\mathcal{N}}_i^p), \end{cases} \tag{9}$$

where $\overrightarrow{\mathcal{N}}_i^p$ denote the set of parent cells of cell i within the power space. The first condition indicates that cell i is damaged if it has been in an overload state for M consecutive steps. The second condition states that cell i fails if its actual workload is below the minimum resource threshold or if its parent cells are damaged or failed. The third condition defines cell i as normal if its actual workload falls between the minimum and overload resource thresholds and its parent cells are either normal or overloaded. The fourth condition indicates that cell i is overloaded if its actual workload exceeds or equals the overload resource threshold and its parent cells are normal or overloaded. Together, these conditions establish the mechanism for simulating the state evolution of power cells in response to cascading failures, resource thresholds, and the influence of neighboring cells.

The water-fire cell state transition rule defines the state change of water-fire cells. Failures in the water-fire cells are influenced by power availability, reflecting the essential role of power in maintaining the functionality of water and fire suppression systems. Additionally, cascading failures within the water-fire system itself are considered, capturing the propagation of disruptions that can lead to system-wide breakdowns in emergency scenarios [46]. The water-fire cell state transition rule for any cell $i \in \mathcal{I}_v$ is defined as:

$$S_{it+1} = \begin{cases} -1, & \text{if } S_{t-M+1} = S_{t-M+2} = \cdots = S_t = 2, \\ 0, & \text{if } (RAWL_{ijt} < RMT_{ij}) \vee (S_{i'jt} = -1 \text{ or } 0, \forall i' \in \overrightarrow{\mathcal{N}}_i^p \cup \overrightarrow{\mathcal{N}}_i^v), \\ 1, & \text{if } (RMT_{ij} \le RAWL_{ijt} < RDT_{ij}) \wedge (S_{i'jt} = 1 \text{ or } 2, \forall i' \in \overrightarrow{\mathcal{N}}_i^p \cup \overrightarrow{\mathcal{N}}_i^v), \\ 2, & \text{if } (RAWL_{ijt} \ge RDT_{ij}) \wedge (S_{i'jt} = 1 \text{ or } 2, \forall i' \in \overrightarrow{\mathcal{N}}_i^p \cup \overrightarrow{\mathcal{N}}_i^v). \end{cases} \tag{10}$$

where $\overrightarrow{\mathcal{N}}_i^v$ denote the set of parent cells of cell i within the water-fire space. The conditions are similar to those of the power cell state transition rule, except that the space for the parent cells is extended to both the power and water-fire cellular spaces. Fig. 2 illustrates the transition process of the cells during system attacks.

3.3. Resilience assessment of power-water-firefighting-space system

This section presents a resilience assessment method for CA-based PWFS systems, focusing on system performance characterization and resilience evaluation. System performance considers structural and functional indicators, while resilience metrics capture key features of the performance curve, including robustness, rapidity, and performance loss.

To assess the resilience of PWFS systems against external perturbations, the first step is to construct the performance curve over time, which is simulated using the enhanced CA model for the PWFS system. Specifically, the system structure is characterized by cellular normality and connectivity, with resource transfer efficiency and functional space normality serving as indicators of system functionality.

Cellular normality (α) is the ratio of the number of cells in the normal state to the total number of cells:

$$\alpha_t = \frac{I_t^{norm}}{I}, \quad \forall t \in \mathcal{T}, \tag{11}$$

where I_t^{norm} denotes the number of cells in the normal state at time t.

Connectivity (β) measures the existence of pathways within the PWFS system that allow the transfer of resources from supply cells to demand cells during the evolution under perturbations. It is calculated as:

$$\beta_t = \frac{1}{I^d} \sum_{i \in \mathcal{I}^d} \left(\frac{1}{J_i^d} \sum_{j \in \mathcal{J}_i^d} \frac{\sum_{l=1}^{t} CP_{ijt}}{l} \right), \quad \forall t \in \mathcal{T}, \tag{12}$$

where $CP_{ijt} = 1$ if a path exists from any supply cell to demand cell i for transferring resource j at time t, and $CP_{ijt} = 0$ otherwise. I^d and $\mathcal{I}^d$ denote the number and set of demand cells, and J_i^d and $\mathcal{J}_i^d$ denote the number and set of resource required by demand cell i. The average connectivity of demand cell i to resource j over time l is computed by $(\sum_{l=1}^{t} CP_{ijt})/l$, and $(\sum_{l=1}^{t} CP_{ijt})/l = 1$ for all $t \in \mathcal{T}$ implying that resource j can always be transferred to demand cell i during the experiment. The average connectivity of all demand cells to resources is then calculated over time t.

Resource transfer efficiency (γ) is the ratio of the quantity of resources consumed by demand cells to the quantity produced by supply cells:

$$\gamma_t = \frac{1}{J} \sum_{j \in \mathcal{J}} \frac{\sum_{i \in \mathcal{I}^d} RAWL_{ijt}}{\sum_{i \in \mathcal{I}^s} RAWL_{ijt}}, \quad \forall t \in \mathcal{T}, \tag{13}$$

where $\mathcal{I}^s$ denotes the set of supply cells.

Functional space normality (δ) is the average residual proportion of each service type within the functional space:

$$\delta_t = \frac{1}{I_s} \sum_{i \in \mathcal{I}_s} \frac{1}{J_i^d} \sum_{j \in \mathcal{J}_i^d} \delta_{ijt}, \quad \forall t \in \mathcal{T}, \tag{14}$$

where I_s and $\mathcal{I}_s$ represent the number and set of cells in the functional space, and $\delta_{ijt} = 1$ for $i \in \mathcal{I}_s$ if cell i in the functional space is in the normal state for resource j at time t, and 0 otherwise.

Since the values of the above-defined indicators lie within the interval $(0, 1)$, this study adopts a linear aggregation method, assuming these indicators are mutually independent, to combine them into a single performance curve over time:

$$P_t = w_1\alpha_t + w_2\beta_t + w_3\gamma_t + w_4\delta_t, \quad \forall t \in \mathcal{T}, \tag{15}$$

where w_k for $k = 1, 2, 3, 4$ are the normalized weight coefficients of the indicators, with $\sum_{k=1}^{4} w_k = 1$. It is straightforward to observe that as $w_1 + w_2 \to 1$, P_t corresponds to the system structure-based characterization, and as $w_3 + w_4 \to 1$, it corresponds to the system functionality-based characterization. The determination of these weights can be made through discussions within an expert panel. It is noteworthy that linear aggregation of indicators is a common method for deriving the performance curve; however, unlike other research, this study provides a theoretical analysis of the sensitivity of this linear aggregation in the later of this section.

Based on the above established performance curve, this study adopts commonly used resilience metrics, including robustness, rapidity, and performance loss, derived from its features during disturbance and recovery periods to assess the resilience of the PWFS system.

Robustness (ROB) is defined as the minimum value of the performance curve during the disturbance and recovery period, representing the absorptive capacity of the PWFS system:

$$ROB = \min_{t \in \mathcal{T}} P_t. \tag{16}$$

Rapidity (RAP) is the ratio of the time taken to reach ROB to the time required to recover from ROB to original performance:

$$RAP = \frac{\arg_{t \in \mathcal{T}}\{P_t = ROB\}}{\arg_{t \in \mathcal{T}}\{P_t = 1\} - \arg_{t \in \mathcal{T}}\{P_t = ROB\}}, \tag{17}$$

where $\arg_{t \in \mathcal{T}} P_t = ROB$ and $\arg_{t \in \mathcal{T}} P_t = 1$ indicate the time steps when the performance curve reaches ROB and fully recovers, respectively.

Performance loss (PL) quantifies the cumulative deviation from original performance over the disturbance and recovery period:

$$PL = \int_0^{\arg_{t \in \mathcal{T}}\{P_t = 1\}} (1 - P_t)\mathrm{d}t. \tag{18}$$

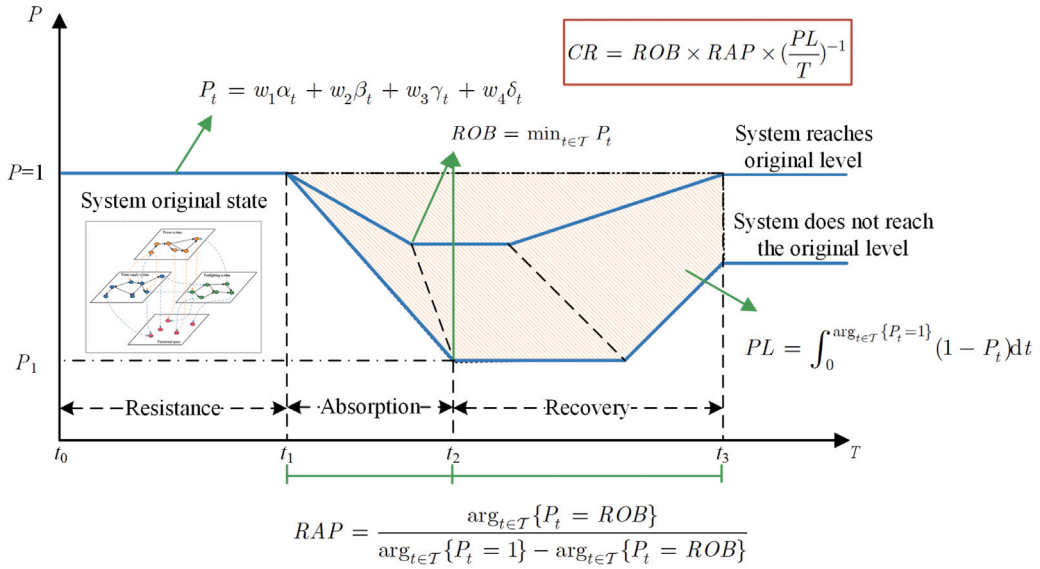

Fig. 3. Schematic of the PWFS system resilience measurement.

A composite resilience indicator (CR) is then constructed by multiplying the three metrics to provide an integrated measure of system resilience:

$$CR = ROB \times RAP \times (\frac{PL}{T})^{-1}. \tag{19}$$

This formulation highlights the positive contributions of ROB and RAP and the negative impact of PL on resilience. The CR metric captures resilience as a dynamic property encompassing absorption, recovery, and adaptation, enabling comparisons across scenarios within the same experimental setting. A schematic of the PWFS system resilience measurement is shown in Fig. 3.

The sensitivity of the resilience of the PWFS system to the weights in the linear aggregation of system performance components is then analyzed. Let Δw_k for $k = 1, 2, 3, 4$ represent the weight variations, and let $\sum_{k=1}^{4} \Delta w_k = 0$ to ensure the normalization of the weights. For simplicity, assign x_t^k for $k = 1, 2, 3, 4$ to α_t, β_t, γ_t, and δ_t. Then, the perturbated performance curve is expressed as:

$$\tilde{P}_t = \sum_{k=1}^{4} (w_k + \Delta w_k) x_t^k, \quad t \in \mathcal{T}. \tag{20}$$

The sensitivity of CR to each resilience metric is approximated using total differentiation, yielding:

$$\Delta CR \approx \frac{\partial CR}{\partial ROB}\Delta ROB + \frac{\partial CR}{\partial RAP}\Delta RAP + \frac{\partial CR}{\partial PL}\Delta PL = CR(\frac{\Delta ROB}{ROB} + \frac{\Delta RAP}{RAP} - \frac{\Delta PL}{PL}), \tag{21}$$

where the second equality follows from that $\frac{\partial CR}{\partial ROB} = \frac{CR}{ROB}$, $\frac{\partial CR}{\partial RAP} = \frac{CR}{RAP}$, and $\frac{\partial CR}{\partial PL} = -\frac{CR}{PL}$. For analytical simplicity, it is reasonable to assume that all resilience metrics reach their respective minimum values at the same point in time. In most cases, the PWFS system experiences its lowest performance level toward the end of the attack phase or shortly thereafter, as cascading failures continue to propagate and overload additional components. Even if certain indicators reach their minimum values earlier, they tend to remain at those levels until the system initiates recovery actions, as observed in case experiments.

For robustness, the following holds:

$$\Delta ROB = \min_{t\in\mathcal{T}} P_t - \min_{t\in\mathcal{T}} \tilde{P}_t = \min_{t\in\mathcal{T}} \{P_t - \tilde{P}_t\} = \sum_{k=1}^{4} \Delta w_k x_{t^*}^k, \tag{22}$$

where t^* denotes the time at which ROB is attained.

For rapidity, $P_t = 1$ if and only if $x_t^k = 1$ for all $k = 1, 2, 3, 4$. Then, the time at which the system returns to its original performance is determined by the slowest-recovering indicator:

$$\arg_{t\in\mathcal{T}}\{\tilde{P}_t = 1\} = \max\left\{\arg_{t\in\mathcal{T}}\{x_t^k = 1\}, k = 1, 2, 3, 4\right\} = \arg_{t\in\mathcal{T}}\{P_t = 1\}, \tag{23}$$

Hence, changes in indicator weights do not affect rapidity.

For performance loss, the following holds:

$$\Delta PL = \int_0^{\arg\{P_t=1\}_{t\in\mathcal{T}}} (1-P_t)\mathrm{d}t - \int_0^{\arg\{P_t=1\}_{t\in\mathcal{T}}} (1-\tilde{P}_t)\mathrm{d}t = \int_0^{\arg\{P_t=1\}_{t\in\mathcal{T}}} \left(\sum_{k=1}^{4}(\Delta w_k x_t^k)\right)\mathrm{d}t = \sum_{k=1}^{4}\Delta w_k \int_0^{\arg\{P_t=1\}_{t\in\mathcal{T}}} x_t^k \mathrm{d}t. \tag{24}$$

Thus, the resulting change in composite resilience is:

$$\Delta CR \approx CR\left(\frac{\sum_{k=1}^{4}\Delta w_k x_{t^*}^k}{ROB} - \frac{\sum_{k=1}^{4}\Delta w_k \int_0^{\arg_{t\in\mathcal{T}}\{P_t=1\}} x_t^k \mathrm{d}t}{PL}\right). \tag{25}$$

This demonstrates that system resilience responds linearly to changes in weights within the aggregated performance curve, despite integrated resilience being derived from the multiplicative aggregation of robustness, rapidity, and performance loss. This linear sensitivity enhances interpretability, facilitating communication with non-technical stakeholders such as policymakers and emergency managers, while also improving model transparency and reducing concerns about bias from weight assignments [47].

3.4. Simulation procedure

This section provides the simulation algorithm for the enhanced CA model for the PWFS system and the corresponding algorithmic complexity analysis to provides the insights into the scalability and computational efficiency.

The following Algorithm 1 presents the simulation procedure of the enhanced CA model for resilience assessment of the PWFS system. The analysis of algorithmic time complexity begins with the time complexity of a single formula. Eq. (7) involves summing over all elements in the neighbor cell set $\mathcal{N}_{i'}$ of a given damaged cell i' under a specific resource j, with a time complexity of $O(N_{i'})$. Eq. (8) sums over all cells in the damaged cell set $\mathcal{I}'$, with a time complexity of $O(I')$. In Eq. (9), the first condition is evaluated M times, while the second, third, and fourth conditions are dominated by the number of parent cells of cell i in the power space, resulting in a time complexity of $\max\{O(M), O(\overline{N}_i^p)\}$. Similarly, for Eq. (10), the time complexity is $\max\{O(M), O(\overline{N}_i^p + \overline{N}_i^v)\}$. The time complexity of Eq. (11) is $O(I)$. Eq. (12), which involves three layers of summation, has a time complexity of $O(I^d \max_{i\in\mathcal{I}^d}\{J_i^d\}t)$. The time complexity of Eq. (13) is $O(J(I^d+I^s))$, while Eq. (14) has a time complexity of $O(I^s \max_{i\in\mathcal{I}^s}\{J_i^d\})$. Notably, since the PWFS system contains the resource of power and water, then $\max_{i\in\mathcal{I}^s}\{J_i^d\} \le 2$ and $\max_{i\in\mathcal{I}^d}\{J_i^d\} \le 2$. Therefore, for the loop in Lines 4–17, the time complexity of Lines 5–15 is:

$$O\left(G\left[\max_{g\in\mathcal{G}}\left\{N_g\left(J(I'+\max_{i\in I'}\{N_{i'}\}) + \max\left\{M, \max_{i\in I_p}\{\overline{N}_i^p\}, \max_{i\in I_v}\{\overline{N}_i^p + \overline{N}_i^v\}\right\}\right)\right\} + \max_{i\in I}\{\overline{N}_i\}\right]\right). \tag{26}$$

The complexity of Line 16 is $O\left(G\left[I + J(I^d + I^s) + I^s\right]\right)$, excluding the time complexity of Eq. (12). The part involving Eq. (12) includes the summation:

$$\sum_{t=1}^{G} O\left(I^d t\right) = O\left(\frac{G(G+1)}{2} I^d\right) = O\left(I^d G^2\right). \tag{27}$$

Thus, the overall time complexity of the perturbation phase is:

$$O\left(G\left[\max_{g\in\mathcal{G}}\{N_g\}\left(I'+\max_{i\in I'}\{N_{i'}\} + \max\left\{M, \max_{i\in I_p}\{\overline{N}_i^p\}, \max_{i\in I_v}\{\overline{N}_i^p + \overline{N}_i^v\}\right\}\right) + \max_{i\in I}\{\overline{N}_i\}\right] + G\left[I + I^d + 2I^s\right] + I^d G^2\right). \tag{28}$$

Through similar analysis, the time complexity of the recover phase is:

$$O\left(I\left[\left(\max_{i'\in\mathcal{H}}\{N_{i'}\}\right)^2 + \max\left\{M, \max_{i\in I_p}\{\overline{N}_i^p\}, \max_{i\in I_v}\{\overline{N}_i^p + \overline{N}_i^v\}\right\}\right] + I^d I^2\right). \tag{29}$$

Overall, the enhanced CA-based resilience assessment algorithm exhibits polynomial complexity, indicating that it can be solved within a reasonable time, with manageable computational costs even as the input size increases, making it suitable for large-scale simulation tasks in practice.

4. Case study

4.1. Case description and data collection

A case study is conducted to demonstrate the proposed enhanced CA-based resilience assessment method, focusing on the outpatient facility at Nanjing Hospital of Traditional Chinese Medicine (NJHTCM). The outpatient building, covering 19,300 square meters, includes a medical space of 44,000 square meters. With an average daily outpatient volume of 2868, the hospital serves a significant number of visitors. Fig. 4 illustrates the exterior views of the outpatient building and its functional areas as shown in the ground floor layout.

The cellular neighborhood of these components is shown in Fig. 5. The power supply of NJHTCM is initially sourced from the municipal grid and then distributed through transformers and power boxes to various end-use facilities, including chillers, lighting, and fire detectors. Similarly, the water supply is routed through components such as storage tanks and pumps to serve both the

Algorithm 1 Simulation Algorithm for Enhanced CA-Based Resilience Assessment

Input: The enhanced CA model of the PWFS system.
Output: Performance curve P, robustness ROB, rapidity RAP, performance loss PL, composite resilience indicator CR, simulation time T.
Initialization: Set of attacked cells $\mathcal{G} := \emptyset$, $t = 0$.
for $t = 1, \ldots, G$ **do**
  Select $g_t \in \mathcal{I} \backslash \mathcal{G}$ by the specific attack pattern, append g_t to $\mathcal{G}$, and set cellular state $S_{g_t} = -1$.
  for $i \in \mathcal{N}_{g_t}$ **do**
    for $j \in \mathcal{J}$ **do**
      Calculate the surplus capacity allocation ΔWL_{ig_tjt} using Equation (7).
      Calculate the actual workload after redistribution $RAWL_{ijt+1}$ using Equation (8).
    end for
    Update the cellular state S_i for power and water-fire cell using Equations (9) and (10).
  end for
  for $i \in \overline{\mathcal{N}}_{g_t}$ **do**
    Set cellular state $S_i = 0$.
  end for
  Calculate the cellular normality α_t, connectivity β_t, resource transfer efficiency γ_t, functional space normality δ_t, and performance P_t using Equations (11)-(15).
end for
while $P_t \neq 1$ **do**
  Select $i' \in \mathcal{I}' := \{i \in \mathcal{I} : S_i = -1\}$ by the specific recovery pattern and append i' to $\mathcal{H}$.
  Set cellular state $S_{i'} = 1$.
  for $i \in \mathcal{N}_i \cup \{i'\}$ **do**
    Calculate the surplus capacity allocation ΔWL_{ig_tjt} using Equation (7).
    Calculate the actual workload after redistribution $RAWL_{ijt+1}$ using Equation (8).
  end for
  Update the cellular state S_i for power and water-fire cell using Equations (9) and (10).
  Calculate the cellular normality α_t, connectivity β_t, resource transfer efficiency γ_t, functional space normality δ_t, and performance P_t using Equations (11)-(15).
  $t \leftarrow t + 1$.
end while
Calculate the robustness ROB, rapidity RAP, performance loss PL, composite resilience indicator CR using Equations (16)-(19).

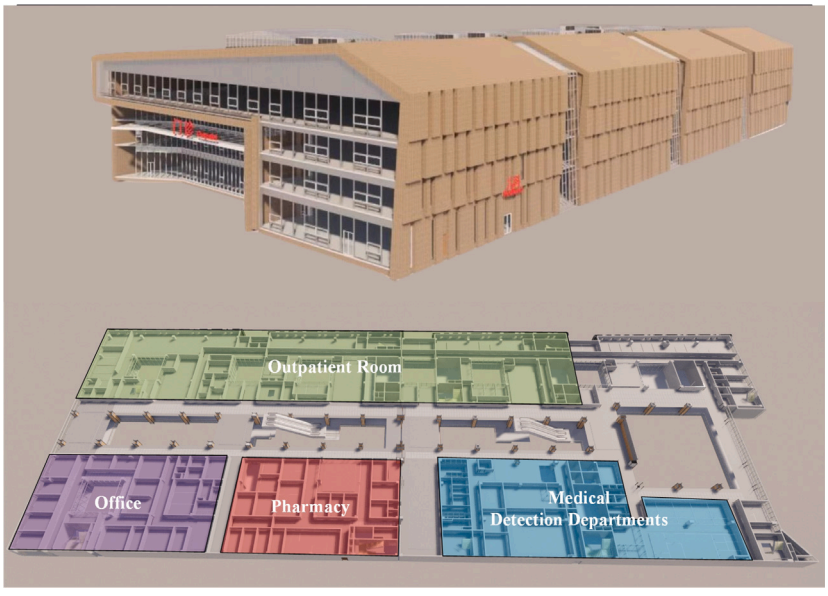

Fig. 4. Exterior views of NJHTCM outpatient building and its functional areas.

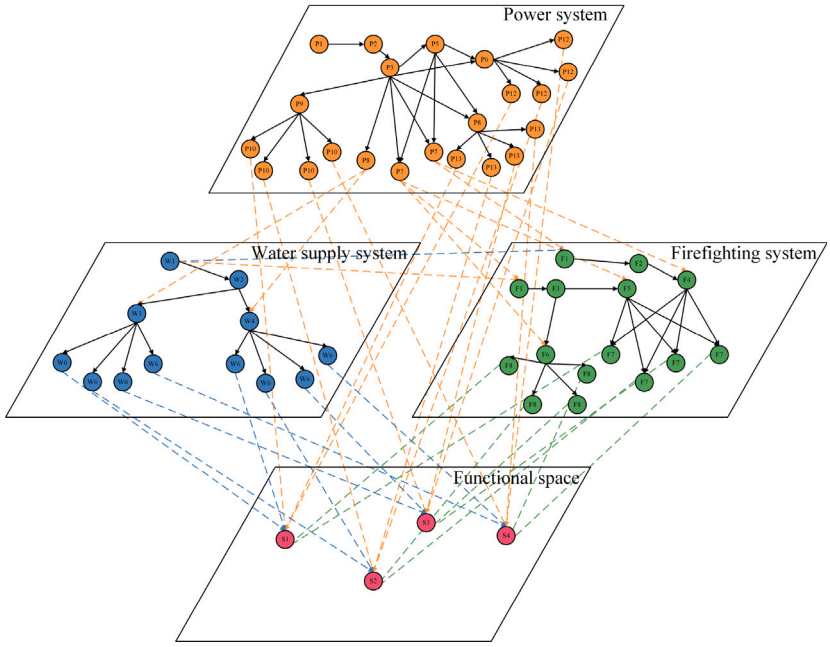

Fig. 5. Cellular neighborhood (interdependency) of the PWFS CA model.

Table 1
Data of daily resource supply and demand among the case PWFS system.

Supply facilities	Target supply	Demand facilities	Target demand
Municipal water supply	2472 (m^3)	Domestic water	1280 (m^3)
		Hot water	400 (m^3)
		Indoor fire hydrant	648 (m^3)
		Fire sprinkler	144 (m^3)
Municipal power supply	16,960 (kWh)	General lighting	4300 (kWh)
		Sockets	1200 (kWh)
		Fire detector	800 (kWh)
		Emergency lighting	600 (kWh)
		Air source heat pump	1200 (kWh)
		Chillers	5500 (kWh)
		Fire transfer pumps	600 (kWh)
		Fire stabilization pumps	1080 (kWh)
		Fire booster pumps	1320 (kWh)
		Sprinkler pressurization pumps	360 (kWh)

hospital and its facilities, including indoor fire hydrants and sprinklers. In the outpatient building (see Fig. 4), functional units include medical detection departments, outpatient rooms, pharmacies, and offices. These units require both hot and cold water for daily use and fire protection, as well as electrical power for outlets, lighting systems, and fire detection equipment. Details of the case PWFS system components and their corresponding identification numbers are provided in Table A.1.

To illustrate the resource dynamics within the PWFS system, this study collects data on resource consumption from the energy audit and building energy efficiency reports of NJHTCM. Table 1 presents an overview of the resource capacity of supply facilities and the resource requirements of demand facilities.

4.2. Simulation setting

The enhanced CA model for the PWFS system includes the following basic settings, which are common in related resilience simulation literature:

(1) Before any disruptions occur, the PWFS system operates in a steady state, with supply, transfer, and demand cells at their normal levels.
(2) The supply cell ensures that the total resource outflow does not exceed its supply capacity.
(3) The number of resources entering the transfer cell equals the number leaving it, indicating that the transfer cell does not consume resources.

Table 2
Simulation parameters.

Parameter	Iteration	Attack ratio	λ	κ	w
Value	100	20%	0.5	1.3	0.25

Table 3
Simulated system resilience results.

System	Simulation results			
	RAP	ROB	PL	CR
PWFS system		0.5577	28.6723	0.2777
Power system	0.3491	0.5547	30.2611	0.2647
Water-fire system		0.5604	27.0644	0.2883

(4) Random attacks affect individual cells, not the links between them.

The overload-to-damage threshold is set at 2; if a cell remains overloaded for two consecutive cycles, it transitions to a failure state in the next cycle. A random attack and recover pattern is used, with an attack ratio of 20%, and the recovery process continued until system performance returned to its pre-attack state. The developed CA model for the case PWFS system consists of 57 cells and 92 links, representing cellular neighborhood relationships. These cells include 2 supply cells, 19 transfer cells, and 47 demand cells. Some cells serve dual functions, such as fire booster pumps, which consume electricity in the power system while also acting as water transfer facilities in the firefighting system. During the weight elicitation for system performance aggregation, three technicians of NJHTCM operations were consulted. As they showed no strong preference among the four performance indicators, equal weights were assigned to each. Using real-world data from the selected hospital, the simulation parameters for this study are summarized in Table 2.

4.3. Case result and analysis

This section analyzes the resilience results of the case PWFS system and further examines the impact of system interdependencies on the overall resilience of the PWFS system.

4.3.1. Resilience analysis

Fig. 6 shows the simulated performance curves for the PWFS system, water-fire system, and power system, respectively. During these experiments, the system experienced four collapses, leading to a total loss of performance. These failures were all caused by municipal power interruptions during the simulation. Notably, the mean performance for all three systems reaches its lowest point at time 12. Excluding collapse scenarios, the performance values for the PWFS, power, and water-fire systems are 0.1370, 0.1213, and 0.1556, respectively.

Table 3 presents the resilience metrics for the PWFS, power, and water-fire systems. The hospital PWFS system shows a mean RAP of 0.3491. For ROB, values range from 0.5547 to 0.5604, with the water-fire system exhibiting the highest value of 0.5604, while the power system is slightly lower at 0.5547. This indicates that the water-fire system is more stable and less affected by uncertainty and external disruptions. The PL analysis shows the power system performs poorly, with a score of 0.7447, indicating it is most vulnerable to disturbances. Regarding the integrated metric CR, the water-fire system has the highest value of 0.2883, while the PWFS and power systems have values of 0.2777 and 0.2647, respectively. Based on the CR distribution, the power system shows lower median and first quartile values compared to the other two systems. As a result, the power system exhibits lower resilience, making it more prone to failure under stress.

4.3.2. Effect of system interdependencies on resilience

Fig. 6(d) illustrates the performance trends of the PWFS, power, and water-fire systems, which show similarities, suggesting a degree of interdependence among these systems. To explore the effect of system interdependence on resilience, this section develops linear regression models for PL and CR across these systems. Examining the resilience interdependence of the PWFS and its subsystems is crucial for optimizing resource allocation and system design. Specifically, if a strong correlation exists between the resilience of different systems, it is essential to account for their interactions when allocating resources to maximize efficiency. Additionally, when designing or improving a system, the interrelationship with other systems must be considered to ensure overall coordination. This study assesses the impact of interdependence on system resilience using the Pearson correlation coefficient and the slope of the fitted trendline. The Pearson correlation coefficient quantifies the strength of the linear relationship between two variables, ranging from −1 to 1, with higher absolute values indicating stronger correlations. The slope of the fitted trendline reflects the coupling strength, where a steeper slope indicates a stronger coupling. The linear regression and correlation analysis of PL and CR jointly reveal the interdependence characteristics of system resilience and performance under perturbations. Specifically, the linear regression of PL reflects the performance correlation under disturbances, while the analysis of CR, incorporating standardized resilience metrics in a non-differentiated scenario, highlights the internal coupling and interdependence of resilience across systems. The macro-level linear fitting analysis of CR further illustrates how system coupling affects overall resilience. Meanwhile, the

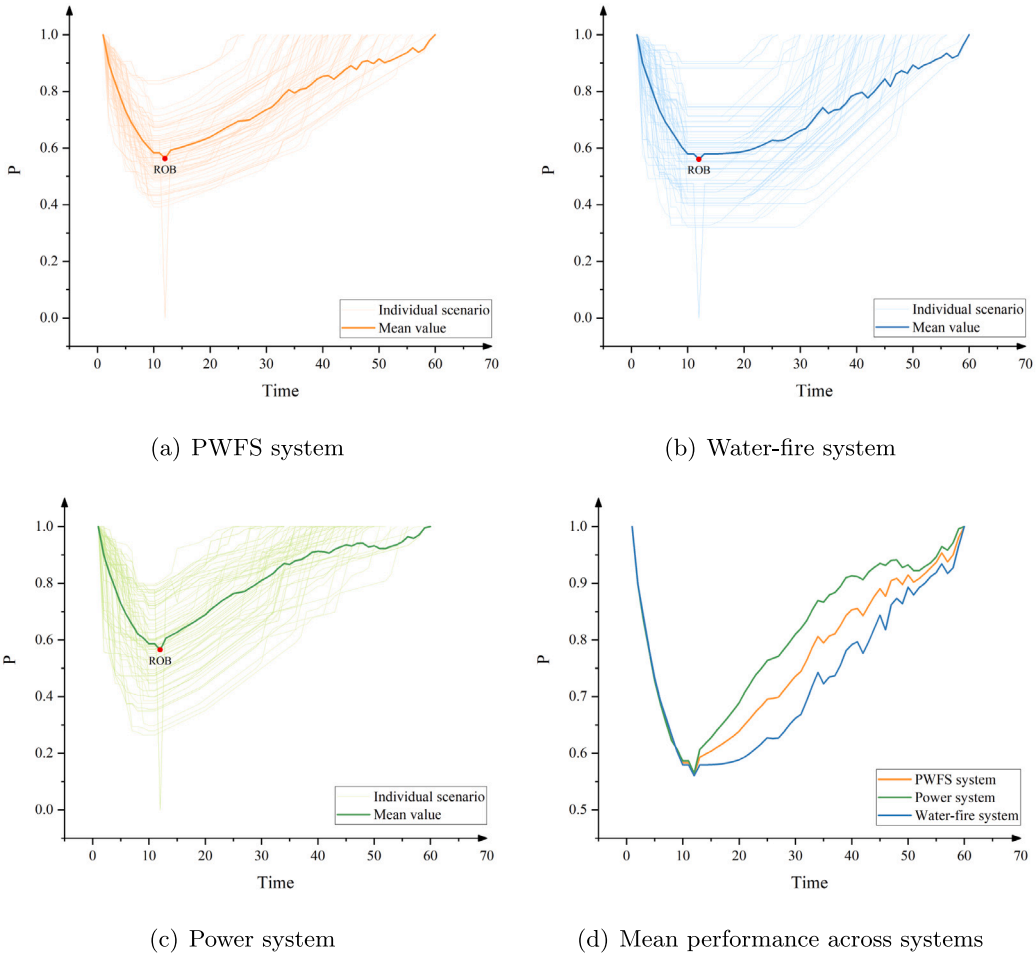

Fig. 6. Simulated system performance curves.

Table 4
PL regression results.

Independent variable	Dependent variable	Pearson's r	Slope	Intercept
PL_{Power}	$PL_{\text{Water-fire}}$	0.4193	0.3809 ± 0.0833	15.5400 ± 2.5685
$PL_{\text{Water-fire}}$	PL_{Power}	0.4193	0.4616 ± 0.1010	17.7687 ± 2.7857
PL_{Power}	PL_{PWFS}	0.8600	0.6918 ± 0.0415	7.7392 ± 1.2783
$PL_{\text{Water-fire}}$	PL_{PWFS}	0.8238	0.7295 ± 0.0507	8.9293 ± 1.399

correlation analysis of PL shows the influence of inter-system dependencies on performance fluctuations. This dual-perspective approach offers a more comprehensive understanding of system resilience from both performance and structural interdependence dimensions.

Table 4 shows that the correlation between the power and water-fire systems is 0.4193, with a trendline slope of 0.3809, indicating a weak correlation in system performance under perturbation. However, a strong positive linear correlation exists between the power system and the PWFS, as well as between the water-fire and PWFS systems, with Pearson correlation coefficients of 0.8600 and 0.8238, respectively. Although the enhanced CA model suggests physical connections between the power and water-fire systems, their simulated PL values appear to be less relevant. This discrepancy may result from cascade failures occurring only in specific scenarios, such as pump damage.

Based on Fig. 7, both CR_{Power} and $CR_{\text{Water-fire}}$ exhibit a strong correlation with CR_{PWFS}, with Pearson correlation coefficients of 0.9872 and 0.9890, respectively. Compared to the water-fire system, the power system (trendline slope = 0.9827) shows a stronger coupling with the PWFS system. To explore the resilience enhancement strategy based on resilience interdependence, this study examines how the resilience of the PWFS system changes when the resilience of the power system and the water-fire system is increased by 1 unit. For example, the resilience increase of the power system by 1 unit is determined by evaluating the corresponding increase in the resilience of the water-fire system, based on the linear fitting results in Fig. 7(a). The enhanced resilience values of the

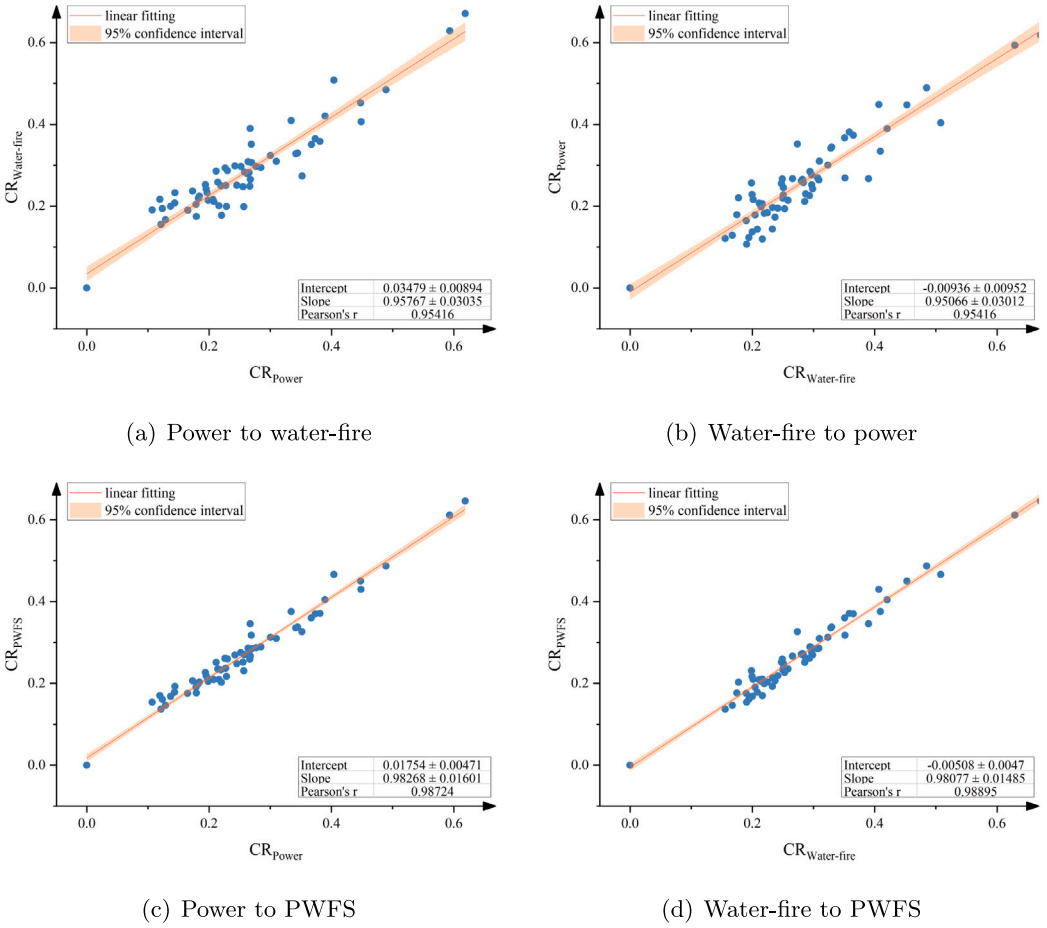

Fig. 7. CR regression results.

power and water-fire systems are then incorporated into the linear fitting equations in Figs. 7(c) and 7(d), respectively. Ultimately, the total resilience enhancement of the PWFS system is the sum of the increases attributed to the power and water-fire systems. Following this approach, the total resilience increases of the PWFS system are 1.9685 units and 1.9182 units for the power and water-fire systems, respectively. Therefore, with limited resources for strengthening the resilience of the PWFS system, prioritizing the enhancement of the resilience of the power system is more effective than focusing on the water-fire system.

4.4. Test of COVID-19 pandemic disturbance

This section presents another real-world test of NJHTCM under the COVID-19 pandemic scenario to further examine the impact of resource surges on system resilience. Based on resource demand data from the COVID-19 period, all functional units, including outpatient rooms, medical detection departments, and offices, experienced a daily increase in water and hot water demand by 12.3% and 30%, respectively, compared to pre-pandemic conditions. Additionally, the electricity demand for sockets in medical detection departments and outpatient rooms rose significantly by 28.6%. As a result, total electricity demand increased by 5.9%, and total water demand for the outpatient building of NJHTCM rose by 8.5%. Furthermore, the simulation maintained the same parameters as the non-pandemic scenario (as shown in Table 2), given that the facility structure of the case PWFS system did not change during the epidemic.

Based on the data changes and simulation parameters, 100 stochastic simulations of the PWFS system under the COVID-19 pandemic scenario are conducted, with results presented in Table 5. Fig. 8 illustrates the time slices of the cellular state evolution in a PWFS system from one experiment, with iteration 29. Throughout these 100 randomized experiments, the system experienced 5 crashes, attributed to abnormalities in municipal power or water supply, a cause similar to that in non-epidemic conditions. The outcomes reveal that CR of the PWFS system and its subsystems has declined to varying extents in the epidemic state, with the power system witnessing the most significant reduction of 19.07% in CR. Meanwhile, ROB of the power system have experienced notable declines of 11.04%, indicating its heightened susceptibility to extreme situations during epidemic conditions. The water-fire

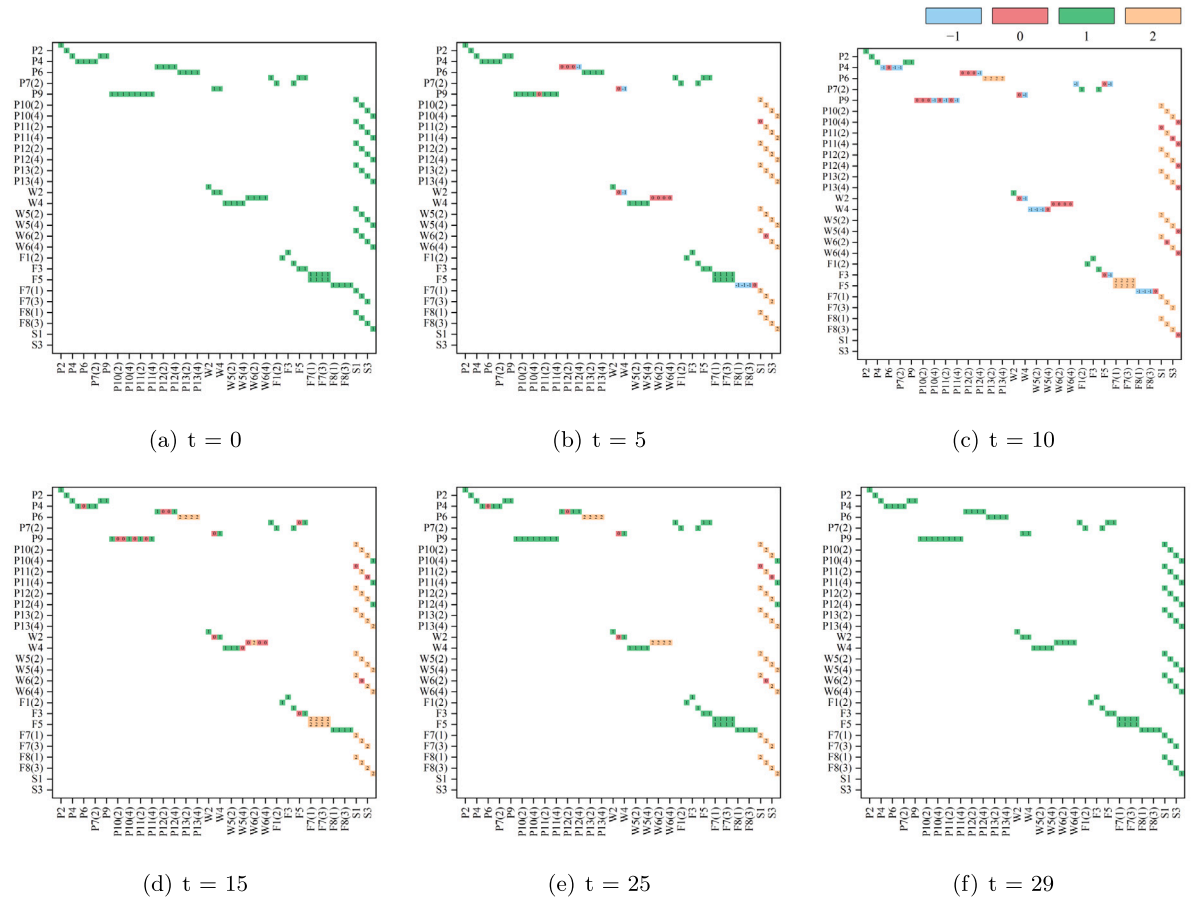

Fig. 8. Time slices of the cellular state evolution.

Table 5
Simulated system resilience results under epidemic scenario.

	RAP	*ROB*	*PL*	*CR*		
				Mean	Median	Quartile
PWFS system		0.5194	29.8907	0.236	0.2887	0.2328
Power system	0.3101	0.4934	30.5174	0.2177	0.2736	0.2133
Water-fire system		0.5526	29.2847	0.2714	0.3065	0.2462

system exhibited the greatest increase in PL at 8.2% during the epidemic state, although the power system retained the highest PL. Moreover, RAP also decreased from 0.3491 to 0.3101, marking an 11.18% decline.

This section also investigates the interdependence effects of the system on resilience in the context of the COVID-19 pandemic, with findings presented in Table 6. The Pearson's correlation coefficient between the power and water-fire systems is calculated at 0.9061, reflecting a 5.03% decrease compared to the pre-pandemic state. Similarly, the coupling strength between these two systems declined by 5.24% and 4.82%, respectively. For each system individually, the correlation coefficients with the PWFS system resilience decreased but remained above 0.9700. Notably, the coupling strength between the power and water-fire systems for the PWFS system resilience shifted from a configuration where the power system's coupling strength was higher to one where the water-fire system now has greater coupling strength, at 0.9623. In the epidemic simulation, as in the non-epidemic scenario, both the power system and water-fire system are assumed to experience a one-unit increase in resilience. The impact of this improvement on the PWFS system shows resilience gains of 1.9023 for the power system and 1.8395 for the water-fire system, indicating reduced efficiency compared to the non-epidemic scenario.

These findings underscore that during the COVID-19 pandemic, the increased demand on hospital power, water, and firefighting systems negatively affected their resilience, making them more vulnerable to stress and disruptions. This surge in demand has also weakened system interdependencies, complicating effective resource allocation and emergency response. Specifically, during the pandemic, the systems faced greater resource demand, and this expansion may have exceeded initial design capacity, resulting

Table 6
CR regression results under epidemic scenario.

Independent variable	Dependent variable	Pearson's r	Slope	Intercept
PL_{Power}	$PL_{\text{Water-fire}}$	0.9061	0.9075 ± 0.0428	0.0537 ± 0.0102
$PL_{\text{Water-fire}}$	PL_{Power}	0.9061	0.9048 ± 0.0427	−0.0097 ± 0.0115
PL_{Power}	PL_{PWFS}	0.9710	0.9552 ± 0.0237	0.0280 ± 0.0056
$PL_{\text{Water-fire}}$	PL_{PWFS}	0.9797	0.9623 ± 0.0199	−0.0058 ± 0.0053

Table 7
Simulated system resilience results across attack patterns.

Attack	PWFS system		Power system		Water-fire system	
	Power	Water-fire	Power	Water-fire	Power	Water-fire
RAP	0.2922	0.4248	0.2922	0.4248	0.2922	0.4248
ROB	0.5862	0.6333	0.3929	0.8862	0.7794	0.3779
PL	30.5301	24.7927	25.508	30.8585	35.5526	18.6146
CR	0.2694	0.3762	0.2161	0.4231	0.3050	0.2975

in decreased interdependencies and inefficient mutual support. Additionally, the increased strain on all systems could expose vulnerabilities. For example, if the water supply system can meet demand under normal conditions but struggles during periods of heightened demand, it could initiate a chain reaction affecting other systems. To ensure hospitals maintain high resilience during a pandemic, comprehensive planning and resource management are essential to ensure coordination and balance across systems.

4.5. Model validation

This section validates the enhanced CA-based resilience assessment for the PWFS system through sensitivity and comparison analysis. The sensitivity analysis considers attack patterns and overload-to-damage thresholds, while the comparison analysis contrasts the performance of the enhanced CA-based assessment with the network-based approach.

4.5.1. Model analysis of attack patterns and overload-to-damage thresholds

The overload-to-damage threshold and attack pattern settings of the enhanced CA model are considered strong assumptions; therefore, model validation for these aspects is provided. Regarding attack patterns, this section examines the resilience results of the PWFS system under random attacks, with the power system and the water-fire system as targets, respectively. For the overload-to-damage threshold, various thresholds are tested. Other specific attack pattern settings, such as those based on network metrics, are not considered, as this study focuses on exploring the resilience characteristics of the PWFS system and the interdependent impact on it.

Simulation results under two representative attack patterns (targeting the power and water-fire systems, respectively) show that the model can differentiate the resilience characteristics of the PWFS system and its subsystems, capturing cascading effects induced by damage. Specifically, the resilience simulation results in Table 7 reveal significant differences in ROB, RAP, PL, and CR for the PWFS system and its subsystems under different attack patterns. When the target is the water-fire system, the PWFS system exhibits higher RAP (0.4248) and ROB (0.6333), with lower PL (24.7927), resulting in a higher CR (0.3762), indicating stronger adaptability and recovery capacity. In contrast, when the power system is targeted, both ROB and CR of the PWFS system decrease significantly to 0.5862 and 0.2694, respectively, suggesting the critical role of the power system within the coupled system, where its damage causes a greater performance impact on the overall system. Further analysis of subsystem performance shows that when the power system is attacked, its ROB (0.3929) and CR (0.2161) are significantly lower than those of the water-fire system under the same attack ($ROB = 0.7794$, $CR = 0.3050$), indicating the weaker resilience of power system. However, when the water-fire system is attacked, the resilience indicators of the power subsystem surpass those of the water-fire system (CR: 0.2975 vs. 0.4231), demonstrating that the power system is more stable under non-targeted attacks. These results confirm the effectiveness of enhanced CA model in identifying key subsystems and assessing resilience characteristics.

Fig. 9 illustrates that as the overload-to-damage threshold increases, the resilience metrics of the PWFS system and its subsystems improve, indicating a greater capacity to withstand prolonged overloads. In terms of ROB, the PWFS system, power system, and water-fire system show consistent improvements, with the power system experiencing an increase from 0.4156 to 0.4735, reflecting enhanced resistance to initial shocks. The PL of the PWFS system decreases from 13.6337 to 12.8535, while the power system shows a more significant reduction in PL, from 12.3509 to 11.2739, suggesting faster recovery after disruptions. CR also increases across all systems, with the CR of PWFS system rising from 0.3170 to 0.3968, and a particularly notable increase in the CR of power system, which reaches 0.5505. These findings confirm the validity of the overload-to-damage threshold settings in the enhanced CA model, demonstrating that higher thresholds effectively reduce structural damage caused by overloads and enhance resilience during dynamic failures and recovery.

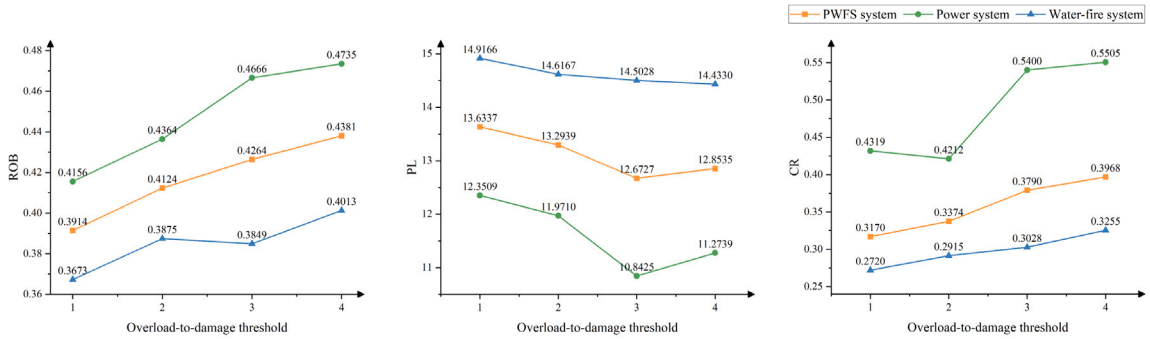

(a) Mean ROB results (b) Mean PL results (c) Mean CR results

Fig. 9. Simulated system resilience results across overload-to-damage thresholds.

Table 8
Network-based resilience metrics and referenced literature.

Indicator	Indicator direction	Literature
Average closeness centrality	Positive	R1
Average betweenness centrality	Positive	R2
Average eigenvector centrality	Positive	R1, R4
Natural connectivity	Positive	R3
Network efficiency	Positive	R1, R2, R3, R4
Largest connected component	Positive	R2
K-core	Positive	R2

Note: R1 [48], R2 [49], R3 [22], R4 [50].

Table 9
Simulated resilience results across comparison benchmarks.

	Our model	R1	R2	R3	R4	E
ROB	0.4135	0.6945	0.8149	0.3216	0.7312	0.6731
PL	12.4158	5.6133	3.3331	17.6948	5.0152	7.5363
CR	0.3667	1.3323	2.6790	0.1895	1.5739	0.9360

4.5.2. Comparison analysis with network-based approach

To enhance the credibility of the proposed enhanced CA model, this section conducts a comparison validation with well-established network-based infrastructure resilience assessment methods. Although agent-based models are commonly used for resilience analysis, they are excluded here due to their dependence on detailed agent behavior design, which varies significantly across systems and undermines cross-model comparability. In contrast, network-based methods offer a more consistent structural representation and are better aligned with the cellular spaces and neighborhood of the enhanced CA model. This alignment enables a meaningful comparison through the enhanced cellular evolution network approach.

Representative literature and associated network-based resilience metrics (as listed in Table 8) are selected for benchmarking. A total of 100 simulations are conducted. In each simulation, multiple network metrics are calculated and aggregated with equal weight to evaluate overall system resilience. To integrate these multiple indicators into a single comparative reference, an aggregated benchmark (denoted as E) is constructed by combining all normalized network metrics, using their initial values as denominators to address scale differences.

Fig. 10 illustrates the resilience curves for system performance under different methods. Table 9 presents the corresponding PWFS system resilience evaluation results. The trends across various models are generally consistent, validating the rationality of the enhanced CA model. The resilience curve of enhanced CA model lies between the E and R3 benchmarks. Notably, ROB observed for R1, R2, R4, and E remain above 0.65, indicating relatively conservative degradation. In contrast, the proposed model and R3 exhibit more significant performance drops, with ROB of 0.4135 and 0.3216, respectively, highlighting their sensitivity to disruptions.

Furthermore, Pearson correlation analysis based on resilience indicators, in Fig. 11, demonstrates that the proposed model maintains strong correlations with most benchmarks, except for R2, which exhibits a lower correlation coefficient of 0.698 and consistently shows weaker correlation with other models as well. In conclusion, the comparative analysis confirms that the proposed enhanced CA model produces resilience evaluation results that are consistent with those of established network-based methods. Despite not employing agent-based models due to their limited comparability, the strong alignment with network-based benchmarks substantiates the reliability of the proposed model.

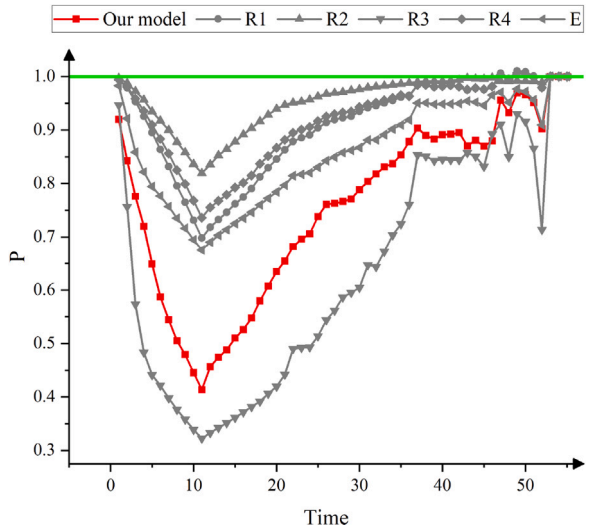

Fig. 10. Simulated system performance curves across comparison benchmarks.

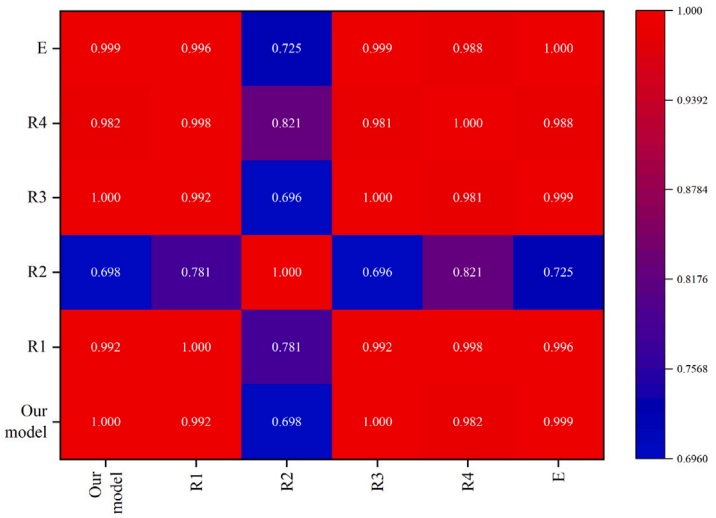

Fig. 11. Correlation heat map of simulated resilience results across comparison benchmarks.

5. Conclusion

This study introduces a novel enhanced CA-based modeling framework to evaluate the resilience of the hospital PWFS system, advancing current research by addressing the limitations of existing methods in capturing the dynamic and interconnected nature of such critical infrastructure. The novelty lies in the formal representation of the PWFS system as a seven-tuple CA model, which enables a fine-grained simulation of system components, their spatial relationships, and the evolution of their states under perturbations. Unlike traditional models, this approach integrates system-level interdependencies, fault propagation mechanisms, and cascading effects into a unified simulation framework. Moreover, by establishing resilience metrics grounded in cellular normality, connectivity, resource transfer efficiency, and functional space normality – alongside system robustness, rapidity, and performance loss – this research provides a quantifiable and systematic method to assess resilience performance. A case study of the outpatient building at NJHTCM in China demonstrates the proposed model, analyzing normal and epidemic scenarios, various attack patterns, parameter variations, and providing a comparative analysis with other network-based resilience assessment methods. These innovations not only offer a new lens through which to understand the operational behavior of hospital lifeline systems under stress but also contribute to the broader body of resilience modeling by bridging the gap between theoretical modeling and real-world emergency scenarios.

The research findings offer valuable insights into the resilience design of hospitals. For power systems, during non-pandemic periods when performance is inadequate, hospital management should prioritize resilience design. This can be achieved by

Table A.1
Components of PWFS system for NJHTCM outpatient building.

ID	Facility	ID	Facility
P1	Municipal electricity supply	W4	Chiller
P2	Transformer	W5	Daily water
P3	Power supply box	W6	Hot water
P4	Fire-fighting electric main distribution box	F1	Fire transfer pump
P5	Fire distribution box	F2	Rooftop fire water tank
P6	Emergency lighting distribution box	F3	Indoor fire storage tank
P7	Fire pump distribution box	F4	Fire stabilization pump
P8	Water pump distribution box	F5	Fire-fighting booster pump
P9	Lighting and socket distribution box	F6	Spray pressurization pump
P10	General lighting	F7	Indoor fire hydrant
P11	Socket	F8	Automatic sprinkler
P12	Fire detector	S1	Outpatient room
P13	Emergency lighting	S2	Medical technology department
W1	Municipal water supply	S3	Pharmacy
W2	Domestic water storage tank	S4	Doctor office
W3	Air source heat pump		

optimizing power supply equipment, strengthening backup power sources, and establishing emergency power recovery plans to ensure reliable power during crises. Additionally, considering the interdependencies between the water-fire and PWFS systems, enhancing the coupling between these two systems can improve overall resilience. For example, adopting mutually supportive design principles to ensure the water-fire system operates effectively is essential for the PWFS system, while optimizing resource allocation and emergency response capabilities across both systems. Finally, hospital management should regularly conduct comprehensive resilience assessments to understand the interdependencies and coupling strength among subsystems, facilitating the development of long-term strategies to enhance hospital resilience and ensure swift response and adaptability in the face of challenges. These insights are critical for improving hospital resilience, reliability, and adaptability in responding to emergencies.

While the proposed enhanced CA model has shown potential in simulating the dynamics of the current PWFS system, its scalability to other interdependent infrastructure systems requires further exploration. The general framework may be extendable, but challenges arise due to system-specific operational mechanisms, dependency structures, and recovery characteristics. Nevertheless, the proposed modeling approach, especially the construction logic based on seven key elements, offers a modular and flexible structure that supports such extensions. To support such scalability, future work should focus on refining the operational mechanisms and state transition rules through the integration of empirical data. For example, incorporating a direct current power flow model could improve the fidelity of power system representations, while embedding recovery strategies that consider real-world constraints, such as limited resources and logistical inefficiencies, would enhance the relevance for resilience planning. By adjusting the state transition rules to reflect the operational characteristics of the target system and reconfiguring the model according to the seven-element framework, the enhanced CA model can be adapted to systems like transportation-communication networks or cyber–physical infrastructures. In addition, future research could further explore key factors influencing the resilience of the PWFS system, such as the number of supply units and the configuration of system redundancies, which would offer valuable insights for the resilience-oriented design of hospital PWFS systems.

CRediT authorship contribution statement

Renlong Wang: Writing – original draft, Conceptualization, Methodology, Software, Formal analysis, Visualization. **Lingzhi Li:** Supervision, Writing – review & editing, Validation, Funding acquisition, Investigation. **Wenjie Lin:** Writing – review & editing. **Endong Wang:** Writing – review & editing, Validation, Methodology. **Jingfeng Yuan:** Writing – review & editing, Funding acquisition.

Funding

This work was supported by National Social Science Foundation of China (No. 24BGL297).

Declaration of competing interest

The authors declare that they have no known competing financial interests or personal relationships that could have appeared to influence the work reported in this paper.

Appendix

See Table A.1.

Data availability

Data will be made available on request.

References

[1] R. Wang, E. Wang, L. Li, W. Li, Evaluating the effectiveness of the covid-19 emergency outbreak prevention and control based on CIA-ISM, Int. J. Environ. Res. Public Heal. 19 (12) (2022) http://dx.doi.org/10.3390/ijerph19127146.

[2] R. Wang, A hybrid MADM method considering expert consensus for emergency recovery plan selection: Dynamic grey relation analysis and partial ordinal priority approach, Inform. Sci. 677 (2024) 120784, http://dx.doi.org/10.1016/j.ins.2024.120784.

[3] R. Wang, R. Shen, S. Cui, X. Shao, H. Chi, M. Gao, Multi-attribute decision-making approach for improvisational emergency supplier selection: Partial ordinal priority approach, Expert Syst. Appl. 288 (2025) 128196, http://dx.doi.org/10.1016/j.eswa.2025.128196.

[4] S. Shady, S. Ahmad, E.-D. Wael, T. Michael, Probabilistic resilience-guided infrastructure risk management, J. Manag. Eng. 36 (6) (2020) 04020073, http://dx.doi.org/10.1061/(ASCE)ME.1943-5479.0000818.

[5] S. Dhakal, L. Zhang, A social welfare–based infrastructure resilience assessment framework: Toward equitable resilience for infrastructure development, Nat. Hazards Rev. 24 (1) (2023) 04022043, http://dx.doi.org/10.1061/(ASCE)NH.1527-6996.0000597.

[6] E.M. Hassan, H. Mahmoud, An integrated socio-technical approach for post-earthquake recovery of interdependent healthcare system, Reliab. Eng. Syst. Saf. 201 (2020) 106953, http://dx.doi.org/10.1016/j.ress.2020.106953.

[7] A. Poudel, S. Argyroudis, K. Pitilakis, Systemic seismic risk assessment of urban healthcare system considering interdependencies to critical infrastructures, Int. J. Disaster Risk Reduct. 103 (2024) 104304, http://dx.doi.org/10.1016/j.ijdrr.2024.104304.

[8] R. Wang, S. Cui, M. Gao, Systematic scenario modeling for priority assessment of sustainable development goals in China under interaction and uncertainty, Environ. Dev. Sustain. (2024) http://dx.doi.org/10.1007/s10668-024-04526-4.

[9] J. Choi, A. Deshmukh, N. Naderpajouh, M. Hastak, Dynamic relationship between functional stress and strain capacity of post-disaster infrastructure, Nat. Hazards 87 (2) (2017) 817–841, http://dx.doi.org/10.1007/s11069-017-2795-5.

[10] J. Liu, C. Zhai, P. Yu, A probabilistic framework to evaluate seismic resilience of hospital buildings using Bayesian networks, Reliab. Eng. Syst. Saf. 226 (2022) 108644, http://dx.doi.org/10.1016/j.ress.2022.108644.

[11] Y. Yang, S.T. Ng, N. Li, X. Xu, P. Xu, F.J. Xu, Adapting HLA-based co-simulation for interdependent infrastructure resilience management, Autom. Constr. 150 (2023) 104860, http://dx.doi.org/10.1016/j.autcon.2023.104860.

[12] H. Mahmoud, T. Kirsch, D. O'Neil, S. Anderson, The resilience of health care systems following major disruptive events: Current practice and a path forward, Reliab. Eng. Syst. Saf. 235 (2023) 109264, http://dx.doi.org/10.1016/j.ress.2023.109264.

[13] Y. Cheng, E.A. Elsayed, Z. Huang, Systems resilience assessments: A review, framework and metrics, Int. J. Prod. Res. 60 (2) (2022) 595–622, http://dx.doi.org/10.1080/00207543.2021.1971789.

[14] L. Li, S. Liao, J. Yuan, E. Wang, J. She, Analyzing healthcare facility resilience: scientometric review and knowledge map, Front. Public Heal. 9 (2021) 764069, http://dx.doi.org/10.3389/fpubh.2021.764069.

[15] F. Haghpanah, K. Ghobadi, B.W. Schafer, Multi-hazard hospital evacuation planning during disease outbreaks using agent-based modeling, Int. J. Disaster Risk Reduct. 66 (2021) 102632, http://dx.doi.org/10.1016/j.ijdrr.2021.102632.

[16] S. Pei, C. Zhai, J. Hu, Surrogate model-assisted seismic resilience assessment of the interdependent transportation and healthcare system considering a two-stage recovery strategy, Reliab. Eng. Syst. Saf. 244 (2024) 109941, http://dx.doi.org/10.1016/j.ress.2024.109941.

[17] W. Chen, M. Wu, L. Zhang, P. Gardoni, Multi-objective optimization for enhancing hospital network resilience under earthquakes, Int. J. Disaster Risk Reduct. 82 (2022) 103281, http://dx.doi.org/10.1016/j.ijdrr.2022.103281.

[18] M. Bruneau, S.E. Chang, R.T. Eguchi, G.C. Lee, T.D. O'Rourke, A.M. Reinhorn, M. Shinozuka, K. Tierney, W.A. Wallace, D. von Winterfeldt, A framework to quantitatively assess and enhance the seismic resilience of communities, Earthq. Spectra 19 (4) (2003) 733–752, http://dx.doi.org/10.1193/1.1623497.

[19] G.P. Cimellaro, C. Renschler, A.M. Reinhorn, L. Arendt, PEOPLES: A framework for evaluating resilience, J. Struct. Eng. 142 (10) (2016) 04016063, http://dx.doi.org/10.1061/(ASCE)ST.1943-541X.0001514.

[20] J. Mochizuki, A. Keating, W. Liu, S. Hochrainer-Stigler, R. Mechler, An overdue alignment of risk and resilience? A conceptual contribution to community resilience, Disasters 42 (2) (2018) 361–391, http://dx.doi.org/10.1111/disa.12239.

[21] C. Poulin, M.B. Kane, Infrastructure resilience curves: Performance measures and summary metrics, Reliab. Eng. Syst. Saf. 216 (2021) 107926, http://dx.doi.org/10.1016/j.ress.2021.107926.

[22] L. Li, Y. Ding, J. Yuan, W. Ji, J. Zhao, L. Shen, Quantifying the resilience of emergency response networks to infrastructure interruptions through an enhanced metanetwork-based framework, J. Manag. Eng. 38 (5) (2022) 04022047, http://dx.doi.org/10.1061/(ASCE)ME.1943-5479.0001080.

[23] D. Carraminana, A.M. Bernardos, J.A. Besada, J.R. Casar, Towards resilient cities: A hybrid simulation framework for risk mitigation through data-driven decision making, Simul. Model. Pr. Theory 133 (2024) 102924, http://dx.doi.org/10.1016/j.simpat.2024.102924.

[24] E. Ouda, A. Sleptchenko, M.C.E. Simsekler, How resilient is your emergency department to inflow surges? A novel multidimensional framework for resilience enhancement, Simul. Model. Pr. Theory 142 (2025) 103105, http://dx.doi.org/10.1016/j.simpat.2025.103105.

[25] L. Das, S. Munikoti, B. Natarajan, B. Srinivasan, Measuring smart grid resilience: Methods, challenges and opportunities, Renew. Sustain. Energy Rev. 130 (2020) 109918, http://dx.doi.org/10.1016/j.rser.2020.109918.

[26] L.E. Yang, J. Scheffran, D. Süsser, R. Dawson, Y.D. Chen, Assessment of flood losses with household responses: agent-based simulation in an Urban Catchment Area, Environ. Model. Assess. 23 (4) (2018) 369–388, http://dx.doi.org/10.1007/s10666-018-9597-3.

[27] L. Sun, B. Stojadinovic, G. Sansavini, Agent-based recovery model for seismic resilience evaluation of electrified communities, Risk Anal. 39 (7) (2019) 1597–1614, http://dx.doi.org/10.1111/risa.13277.

[28] D. Carramiñana, A.M. Bernardos, J.A. Besada, J.R. Casar, Enhancing healthcare infrastructure resilience through agent-based simulation methods, Comput. Commun. (2025) 108070, http://dx.doi.org/10.1016/j.comcom.2025.108070.

[29] Y. Yang, H. Liu, S. Zhong, K. Liu, M. Wang, Q. Huang, Agent-based societal impact modeling for infrastructure disruption and countermeasures analyses, Sustain. Cities Soc. 97 (2023) 104737, http://dx.doi.org/10.1016/j.scs.2023.104737.

[30] C. Liu, Y. Yang, H. Liu, J. Hu, Agent-based modeling for estimating the performance of medical service systems in disaster scenarios, Int. J. Disaster Risk Reduct. 117 (2025) 105183, http://dx.doi.org/10.1016/j.ijdrr.2025.105183.

[31] Y. Wu, S. Chen, Traffic resilience modeling for post-earthquake emergency medical response and planning considering disrupted infrastructure and dislocated residents, Int. J. Disaster Risk Reduct. 93 (2023) 103754, http://dx.doi.org/10.1016/j.ijdrr.2023.103754.

[32] M. Taghizadeh, M. Mahsuli, H. Poorzahedy, Probabilistic framework for evaluating the seismic resilience of transportation systems during emergency medical response, Reliab. Eng. Syst. Saf. 236 (2023) 109255, http://dx.doi.org/10.1016/j.ress.2023.109255.

[33] Z. Li, H.W. Lim, N. Li, Y. Long, D. Fang, Assessing the seismic resilience of a healthcare system: A hybrid modeling, Int. J. Disaster Risk Reduct. 93 (2023) 103730, http://dx.doi.org/10.1016/j.ijdrr.2023.103730.

[34] M. Aghababaei, M. Koliou, Community resilience assessment via agent-based modeling approach, Comput.- Aided Civ. Infrastruct. Eng. 38 (7) (2023) 920–939, http://dx.doi.org/10.1111/mice.12916.
[35] W. Bi, K. MacAskill, J. Schooling, Old wine in new bottles? Understanding infrastructure resilience: Foundations, assessment, and limitations, Transp. Res. Part D: Transp. Environ. 120 (2023) 103793, http://dx.doi.org/10.1016/j.trd.2023.103793.
[36] F. Goodarzian, P. Ghasemi, A. Gunasekaren, A.A. Taleizadeh, A. Abraham, A sustainable-resilience healthcare network for handling COVID-19 pandemic, Ann. Oper. Res. 312 (2) (2022) 761–825, http://dx.doi.org/10.1007/s10479-021-04238-2.
[37] L. Li, J. Wang, J. Yuan, T. Gu, S. Ling, H. Zhan, Unlocking physical resilience capacities of building systems: An enhanced network analysis approach, Buildings 15 (4) (2025) 641, http://dx.doi.org/10.3390/buildings15040641.
[38] Y. Li, M. Zhang, Cascading failure analysis of interdependent water-power networks based on functional coupling, Reliab. Eng. Syst. Saf. 259 (2025) 110950, http://dx.doi.org/10.1016/j.ress.2025.110950.
[39] M. Ouyang, Review on modeling and simulation of interdependent critical infrastructure systems, Reliab. Eng. Syst. Saf. 121 (2014) 43–60, http://dx.doi.org/10.1016/j.ress.2013.06.040.
[40] S. Wolfram, Cellular automata as models of complexity, Nature 311 (5985) (1984) 419–424, http://dx.doi.org/10.1038/311419a0.
[41] G.M.B. de Oliveira, S.R.C. Siqueira, Parameter characterization of two-dimensional cellular automata rule space, Phys. D: Nonlinear Phenom. 217 (1) (2006) 1–6, http://dx.doi.org/10.1016/j.physd.2006.02.010.
[42] Y. Li, M. Chen, Z. Dou, X. Zheng, Y. Cheng, A. Mebarki, A review of cellular automata models for crowd evacuation, Phys. A 526 (2019) 120752, http://dx.doi.org/10.1016/j.physa.2019.03.117.
[43] X. Tong, Y. Feng, A review of assessment methods for cellular automata models of land-use change and urban growth, Int. J. Geogr. Inf. Sci. 34 (5) (2020) 866–898, http://dx.doi.org/10.1080/13658816.2019.1684499.
[44] B. Berkowitz, Analysis of fracture network connectivity using percolation theory, Math. Geol. 27 (4) (1995) 467–483, http://dx.doi.org/10.1007/BF02084422.
[45] L. Traynham, R. Palmer, A. Polebitski, Impacts of future climate conditions and forecasted population growth on water supply systems in the Puget Sound Region, J. Water Resour. Plan. Manag. 137 (4) (2011) 318–326, http://dx.doi.org/10.1061/(ASCE)WR.1943-5452.0000114.
[46] S. Wang, X. Li, F. Yu, Dynamic assessment method of urban critical infrastructure system physical interdependency vulnerability, Oper. Res. Manag. Sci. 26 (2017) 115–122, http://dx.doi.org/10.12005/orms.2017.0194.
[47] S. Cui, R. Wang, X. Li, X. Bai, Policy-driven analysis of carbon emission efficiency under uncertainty and its application in Chinese industry: Hybrid delta-slacks-based model and ordinal priority approach, Energy 324 (2025) 135832, http://dx.doi.org/10.1016/j.energy.2025.135832.
[48] H. Xu, B. Li, Y. Wang, Determining the key urban infrastructures in disaster scenarios based on complex network theory, Nat. Hazards (2025) http://dx.doi.org/10.1007/s11069-025-07237-9.
[49] M. Wei, J. Xu, Assessing road network resilience in disaster areas from a complex network perspective: A real-life case study from China, Int. J. Disaster Risk Reduct. 100 (2024) 104167, http://dx.doi.org/10.1016/j.ijdrr.2023.104167.
[50] Z. Chen, S. Zhu, H. Feng, H. Zhang, D. Li, Coupling dynamics of urban flood resilience in China from 2012 to 2022: A network-based approach, Sustain. Cities Soc. 118 (2025) 105996, http://dx.doi.org/10.1016/j.scs.2024.105996.